Numerical study of circulation and temperature-salinity distributions in the Bras d'Or Lakes

Bo Yang[1,2], Jinyu Sheng[1], Bruce G. Hatcher[2] and Brian Petrie[3]

[1]Department of Oceanography, Dalhousie University, Halifax, Nova Scotia, B3H 4J1, Canada

[2]Bras d'Or Institute for Ecosystem Research, Cape Breton University, Sydney, Nova Scotia, B1P 6L2, Canada

[3]Ocean Science Division, Bedford Institute of Oceanography, Dartmouth, Nova Scotia, B2Y 4A2

Keywords: Bras d'Or Lakes, numerical model, process study, density-driven circulation, wind forcing, tides, river runoff

Corresponding author address:
Dr. Jinyu Sheng, Department of Oceanography
Dalhousie University, Halifax, NS, B3H 4J1, Canada
E-mail: Jinyu.Sheng@Dal.Ca
Phone: (902) 494-2718, Fax: (902) 494-2885

(Ocean Dynamics, 2007, in press)

Abstract

The Bras d'Or Lakes (BdOL) are a large, complex and virtually land-locked estuary in central Cape Breton Island of Nova Scotia, and one of Canada's charismatic ecosystems, sustaining ecological and cultural communities unique in many aspects. The BdOL comprise two major basins, many deep and shallow bays, several narrow channels and straits, and a large, geologically complex watershed. Predictive knowledge of the water movement within the estuary is a key requirement for effective management and sustainable development of the BdOL ecosystem. A three-dimensional (3D) primitive-equation ocean circulation model is used to examine the estuary's response to tides, winds and buoyancy forcing associated with freshwater runoff in a series of numerical experiments validated with empirical data. The model results generate intense jet-like tidal flows of about 1 m s^{-1} in the channels between the basins and connecting them to the ocean, and relatively weak tidal currents in other regions, which agrees well with previous observations and numerical results. Wind forcing and buoyancy forcing associated with river runoff play important roles in generating the significant sub-tidal circulations in the estuary, including narrow channels, deep basins and shallow bays. The circulation model is also used to reconstruct the 3D circulation and temperature-salinity distributions in the summer months of 1974, when current and hydrographic measurements were made at several locations. The sub-tidal circulation in the estuary produced by the model is characterized by wind and barometric set-up and set-down in different sections of the system, and a classic two-layer estuarine circulation in which brackish, near-surface waters flow seaward from the estuary into the Atlantic Ocean, and deep salty waters flow landward through the major channel. The model results reproduce reasonably well the overall features of observed circulation and temperature-salinity fields made in the BdOL in 1974, but generally underestimate the observed currents and density stratification. The model discrepancies reflect the use of spatially mean wind forcing and spatially and monthly mean surface heat flux and the inability of the coarse model horizontal resolution (~500 m) to resolve narrow channels and straits.

1 Introduction

The Bras d'Or Lakes (BdOL) are a large, complex and virtually land-locked estuary in central Cape Breton Island of Nova Scotia, Canada. The BdOL have a surface area of about 1100 km^2 and water volume of about 32 km^3 (Petrie and Bugden 2002). The Bras d'Or ecosystem comprises a series of elongated, southwest-to-northeast basins connected by narrow channels, and nested between isolated hills and highlands in a watershed of approximately 3600 km^2 (Taylor and Shaw 2002). The Great Bras d'Or Channel, North Basin, St. Andrew's Channel, Baddeck Bay, St. Patrick's Channel and Whycocomagh Bay form the northern part; and the Bras d'Or Lake, Denys Basin, East Bay and West Bay form the southern part (Fig. 1). The bottom topography in the region is highly variable, with the greatest water depth of about 530 m in the central St. Andrew's Channel and shallow water depth of less than 10 m over extensive areas of the Denys Basin. The BdOL are connected to the North Atlantic Ocean through three distinct passages: the Great Bras d'Or Channel and the Little Bras d'Or Channel to the north, and St. Peter's Canal to the south. The Great Bras d'Or Channel (GBC) is relatively straight, about 30 km long with an average width of about 1.3 km and an average depth of about 19 m. The mouth of the GBC has a sill depth of about 10 m and a narrow opening about 300 m wide. The GBC provides significant interchange between the BdOL and the North Atlantic Ocean via Sydney Bight and the Cabot Strait (Fig. 1).

The Little Bras d'Or Channel is long, narrow, convoluted and shallow, with a mean width of about 100 m and a sill depth of about 5 m. Hence, it plays only a minor role in connecting the BdOL to the North Atlantic Ocean (Gurbutt and Petrie 1995). A pair of locks in St. Peter's Canal on the southern side of the BdOL open sporadically to allow vessels of less than 10 m beam to enter or leave the BdOL, so the water exchange through the canal is very limited and therefore can be ignored for the purposes of this study. The Barra Strait is an inner passage connecting the northern and southern parts of the BdOL with a sill depth of about 20 m and a minimum width of about 500 m (Fig. 1). Salinity in the BdOL is in the range of 20 to 26 psu (practical salinity units), which is lower than the salinity (~28 and 32 psu) in Sydney Bight and Cabot Strait.

The restricted hydrodynamic exchange between the BdOL and the ocean surrounding Cape Breton also limits ecological connections. Fish within the BdOL have very similar characteristics to those along the Canadian Atlantic coast, but comprise a smaller sub-set of species (Lambert 2002). Populations of winter flounder (*Pleuronectes sp.*) and herring (*Harengula sp.*) supported commercial fisheries in the BdOL before the 1990's. The winter flounder fishery ended in 1992 with the barring of commercial draggers from the BdOL, and the spring herring fishery was stopped

in 1999 due to the imminent collapse of the stock. Some invertebrates, including lobsters, oysters, scallops and rock crabs, have also been harvested in the BdOL, among which oysters form the basis of an important fishing and aquaculture industry (Lambert 2002). In October 2000, an oyster parasite known as *Haplosporidium nelsoni* (MSX disease) was discovered in specimens of the American Oyster (*Crassostrea virginica*) at localized sites within the BdOL (Stephenson et al. 2003). The MSX disease kills most of the oysters that become infected. Large numbers of oysters died in the affected areas of the BdOL in 2002, severely disrupting the local oyster industry. Although the MSX disease has been detected mainly in the BdOL to date and is apparently absent from some localized populations there, it threatens oyster aquaculture and fisheries in other littoral communities of Atlantic Canada because the infective life stage is thought to be waterborne and could be dispersed with the ocean circulation over the region (Burreson and Ford 2004). Therefore, there is an urgent need to gain better and reliable knowledge of general circulation and associated hydrodynamic and ecological connectivity in the BdOL (Stephensen and Petrie 2005).

Circulation in the BdOL is affected by tides, wind forcing, sea surface heat and freshwater fluxes. A reader is referred to Petrie and Bugden (2002) for a latest review of current knowledge of main physical processes in the BdOL. Based on oceanographic observations made in the BdOL from 1972 to 1974, Petrie (1999) examined the variability of tidal amplitudes and phases in the BdOL and demonstrated that the M_2 tide is the most dominant constituent among the five principal tidal constituents (M_2, S_2, N_2, K_1 and O_1). Circulation in the BdOL is also affected by buoyancy forcing associated with river runoff. Krauel (1975b) estimated that the freshwater discharge to the BdOL has a maximum of about 300 $m^3 s^{-1}$, which means that the sea level would rise about 2.3 cm per day within the BdOL if the passages connected to the Atlantic Ocean were all closed.

Some numerical modelling efforts were made in the past to study the tidal and density-driven circulation in the BdOL. Gurbutt and Petrie (1995) used a box model with two or three layers in each of nine separate regions, and constructed the summer mean general circulation pattern within the lakes. It consists of a deep inflow from Sydney Bight through the GBC, and a surface outflow that is warmed by solar heating in seasons other than winter, and freshened by precipitation. Petrie (1999) developed a one-dimensional, cross-sectionally averaged model for sea level variability in the BdOL. Petrie's model results demonstrated the tidal and sub-tidal sea level variability in the lakes and the importance of the frictional dissipation in the GBC and Barra Strait. Dupont et al. (2003) developed a two-dimensional (2D, or depth-averaged) finite element model of the tidal circulation for the BdOL, using five principal tidal constituents (M_2, S_2, N_2, K_1 and O_1). Although all of the previous numerical studies were very useful in providing general knowledge of the tidal

and sub-tidal circulation and hydrographic distributions in the BdOL, the three-dimensional (3D) circulation, temperature-salinity distributions, and their associated variability in response to variable forcing, have not been well studied. The main objectives of this study are: (1) to undertake a detailed process analysis of the circulation in response to tides, wind forcing, and river runoff; and (2) to reconstruct the 3D circulation and hydrographic distributions in the BdOL in the summer of 1974 using a primitive-equation, z-level ocean circulation model. The model results are intended for subsequent use in coupled bio-physical models in which the hydrodynamic connectivity among cultivation sites and the spatially-explicit risks of MSX disease spreading in the BdOL and beyond are studied.

The arrangement of this paper is as follows. Section 2 describes the model configurations, external forcing, and model initial conditions used in the numerical experiments. Section 3 presents the process study of the response of the BdOL to tides, steady wind forcing and buoyancy forcing associated with river runoff, and reconstruction of the 3D circulation and hydrographic distributions in the BdOL in the spring and summer of 1974. Section 4 discusses the influence of sub-tidal sea level variations specified at the mouth of the GBC to the circulation within the BdOL. The final section summarizes and discusses the results in the context of previous, similar studies in the BdOL and elsewhere.

2 The hydrodynamic circulation model and external forcing

2.1 The model setup

The circulation model used in this study is the 3D, primitive-equation, free-surface, z-level ocean model known as CANDIE (Sheng et al. 1998). CANDIE has successfully simulated the large-scale circulation in the northwestern Atlantic Ocean (Sheng et al. 2001), tidal circulation in the Gulf of St. Lawrence (Lu et al. 2001), 3D circulation in the Western Caribbean Sea (Sheng and Tang 2003; Tang et al. 2006; Sheng et al. 2007), and circulation and thermal structure in Lake Huron (Sheng and Rao, 2006). The model was also used in process studies of wind-driven circulation over an idealized coastal canyon (Sheng et al. 1998), nonlinear dynamics of the Gaspé Current (Sheng 2001), wind-driven circulation over a stratified coastal embayment (Davidson et al. 2001), storm-induced circulation on the Scotia Shelf during Hurricane Juan (Sheng et al. 2006), and nonlinear tidal dynamics in Lunenburg Bay (Sheng and Wang 2004).

The model domain covers the entire BdOL, with the exception of the Little Bras d'Or Channel and St. Peter's Canal (Fig. 1), at a horizontal resolution of ~500 m. It should be noted that several

narrow straits inside the lakes, such as Barra Strait and Little Narrows, are barely resolved by the current model resolution. To better resolve circulation through these narrow straits, a nested-grid finite difference model used by Sheng et al. (2005) and Sheng et al. (2007), or a finite-element (or finite volume) model could be used. In this study, the BdOL model uses 24 z-levels in the vertical, with a vertical resolution of 4 m for the top z-level, 2 m for the following 17 z-levels and a coarser vertical resolution for the last 6 z-levels. Due mainly to the coarse horizontal resolution, the model does not resolve the Little Bras d'Or Channel and St. Peter's Canal. As a result, the model BdOL is connected to the Atlantic Ocean only through the GBC, with the northern open boundary located at the mouth of the GBC at Table Head Point (Fig. 1). The model time step is set to 35 s, which is 3 times larger than the maximum time step determined by the conventional Courant-Friedrichs-Lewy (CFL) stability criterion (which is less than 11 s), meaning that the circulation model based on CANDIE is computationally very efficient. The model uses the horizontal mixing scheme of Smagorinsky (1963) for the horizontal eddy viscosity coefficient A_m, the modified KPP scheme for the vertical eddy viscosity and diffusivity coefficients K_m and K_h, and a quadratic bottom stress parameterization with a dimensionless drag coefficient set to 3.0×10^{-3}. It should be noted that the original KKP scheme of Large et al. (1994) was developed to approximate the vertical mixing processes in the deep ocean. Durski et al. (2004) modified the KPP scheme by including a representation of the bottom layer response. They demonstrated that model results using the modified KPP scheme compare reasonably well to those using the level-2.5 Mellor-Yamada (1982) scheme in series of idealized continental shelf experiments. In this study, the modified KPP scheme suggested by Durski et al. (2004) is used. At model lateral closed boundaries, we use the no-slip and zero normal flow conditions for horizontal components of currents and zero horizontal flux conditions for temperature and salinity.

2.2 External forcing of the model

Three types of external forcings are used in this study to drive the circulation model of the BdOL: tidal forcing and sub-tidal currents associated with non-isostatic responses to the atmospheric pressure fluctuations at the northern open boundary (boundary forcing); surface wind forcing, heat flux at the sea surface; and buoyancy forcing associated with freshwater runoff from major rivers in the BdOL.

(a) Open boundary conditions (tidal and non-tidal boundary forcing)

We follow Davies and Flather (1978) and specify the tidal and non-tidal boundary forcing at the model's northern open boundary based on

$$u_b = u_t + u_s + \frac{c}{h}(\eta_b - \eta_t - \eta_s) \quad (1)$$

where η_b and u_b are the model-calculated sea surface elevation and normal flow at the model open boundary, η_t and u_t are the tidal input of sea surface elevation and (depth-mean) currents at model open boundary, η_s and u_s are the sea surface elevation and depth-mean currents associated with non-tidal fluctuations at the model open boundary, h is the local water depth, and c is the external gravity wave phase speed.

Since no direct current measurements were made at the model's open boundary (i.e., the mouth of the GBC), we approximate the tidal and non-tidal currents at this open boundary by setting $u_t + u_s = u_{b-1}$, where u_{b-1} is the model-calculated current at grid points closest to the open boundary. We also assume the tidal surface elevation η_t at the open boundary to be spatially uniform, a reasonable approximation since the width of the GBC at the open boundary is only about 5 km, which is very small in comparison with the typical tidal wavelengths of several hundreds to thousands of kilometers.

There were no direct sea level measurements at Table Head to be used in this study. As a result, the tidal surface elevations (η_t) at the northern open boundary are calculated from harmonic constants for the five tidal constituents (M_2, S_2, N_2, K_1 and O_1) estimated by Petrie (1999) at the Point. The time-series of η_t used to drive the model is presented in Fig. 2a, which demonstrates that the M_2 tide, which accounts for ~84% of the total variances of η_t, is the dominant tidal component among the five constituents estimated at the Point. The four other tidal components, S_2, N_2, K_1 and O_1 only account for ~3-5% of the total variances.

The sub-tidal (low frequency) surface elevations do not change much from Sydney Bight to the interior of the BdOL (Petrie and Bugden 2002). For simplicity, we assume that the sub-tidal surface elevations η_s at Table Head Point, outside of the BdOL, are the same as those in North Sydney, and the latter are estimated from the tide gauge data (Fig 2b). Physically, the sub-tidal surface elevations over Sydney Bight are affected by many processes such as the inverse barometer effect associated with atmospheric pressure perturbations, coastal setup due to wind forcing, and sea level variations in the Gulf of St. Lawrence that move into Sydney Bight. To identify main processes responsible for the sub-tidal surface elevations in the Bight, we calculate the sea surface elevations due to the inverse barometer effect (i.e., $\eta_a = -\tilde{p}_a / \rho_o g$, where $\tilde{p}_a$ is the sea-level atmospheric pressure perturbation, ρ_o is the reference density of sea water and g is the Earth's gravitation acceleration)

from the atmospheric pressure measurements at Sydney Airport and compare η_a with the observed sub-tidal surface elevation η_s in the Bight. A comparison of η_s with η_a in Fig. 2b demonstrates that the inverse barometer effect, which accounts for ~73% of the total variance of the non-tidal surface elevations at North Sydney, plays an important role in generating the low-frequency sea level fluctuations in the Bight during the study period.

Petrie and Budgen (2002) suggested that the sub-tidal level variations due to the sea-level atmospheric pressure fluctuations in Sydney Bight play a very important role in driving circulation in the GBC and the BdOL. This is mainly because a high (low) atmospheric pressure system over the Bight and the BdOL region, which usually has typical length scales of hundreds of kilometers, move waters from (to) the Bight much quicker than from (to) the BdOL because the GBC restricts water movement between the BdOL and the Bight. As the atmospheric pressure increases (decreases), the sea level falls (rises) first in Sydney Bight, leaving sea level in the BdOL higher (lower), which generates sea level differences between Sydney Bight and the GBC, and produces currents in the GBC and the BdOL until a new balance is reached (Petrie and Budgen 2002, see also Section 4).

For model temperature and salinity fields, we use adaptive open boundary conditions (Sheng et al. 2005) at the northern open boundary. It first uses an explicit Orlanski (1976) radiation condition to determine whether the open boundary is passive (outward propagation) or active (inward propagation). If the open boundary is passive, the model prognostic variables of temperature and salinity are radiated outward to allow any perturbation generated inside the model domain to propagate outward. If the open boundary is active, the model prognostic variables at the open boundary are specified using the monthly mean hydrographic climatology (Geshelin et al. 1999).

(b) Wind forcing

Due to high elevation land mass surrounding the BdOL, wind fields over the lakes are likely to have many small-scale circulation features resulting from topographic steering. Since there were no direct meteorological measurements available to determine the spatial structures of the wind forcing during the study period, we assume that the wind forcing in the BdOL is spatially uniform and equal to the wind forcing calculated from the wind velocity measurements at Sydney Airport using the bulk formula of Large and Pond (1981). Fig. 2c demonstrates that the observed wind speeds at the Airport have significant temporal variability during the study period, with typical amplitude of about 10 m s^{-1} and periods of 5 to 6 days.

(c) Surface heat flux

The lake surface boundary condition for temperature is given by

$$K_h \frac{\partial T}{\partial z} = \frac{Q}{C_p \rho_0} \tag{2}$$

where C_p is the specific heat capacity of lake water and Q is the net heat flux calculated based on Gill (1982):

$$Q = Q_b + Q_L + Q_s - Q_i \tag{3}$$

where Q_b is the net upward flux of long-wave radiation from the water, Q_L is the latent heat of vaporization of water, Q_s is the upward sensible heat flux, and Q_i is the absorption of solar radiation. Here Q_b, Q_L and Q_s are calculated using some empirical formulas based on the air temperature, relative humidity, wind speed, fraction of sky covered by cloud and model-calculated lake surface temperature (LST). The hourly measurements of air temperature and relative humidity at Sydney Airport are used in the calculation of heat fluxes. Since there were no direct observations of solar radiation available at Sydney Airport, the BdOL or adjacent regions in 1974, monthly averaged insolation extracted from the Surface meteorology and Solar Energy (SSE, see http://eosweb.larc.nasa.gov/sse) 10-year dataset are used and assumed to be uniformly distributed throughout the model domain. The SSE dataset was derived from the NASA Earth Science Enterprise (ESE) program's satellite and reanalysis research data.

(d) Freshwater runoff

A large quantity of fresh water isdischarged into the BdOL from several rivers and brooks, which significantly affects the density-driven circulation in the BdOL. We follow Krauel (1975b) and estimate the monthly mean freshwater input during the study period by calculating the monthly discharge per km^2 of the catchment area from the four gauging stations around the BdOL and multiplying this value by the catchment area of the entire watershed. The monthly mean freshwater discharge of four gauging stations in 1974 and the estimated input to the BdOL are listed in Table 1, with an estimated accuracy of ±25% (Krauel 1975b). The whole watershed of the BdOL is divided into 12 sub-watersheds according to the BdOL Watershed Chart (Johnson 2004). The freshwater discharge from each sub-watershed is specified based on the fraction of its catchment area to that of the Lake System. Only one or two large rivers in each sub-watershed are considered, through which all freshwater of this sub-watershed are assumed to discharge into the BdOL. There are 17 major

rivers specified in the model (see Fig. 1 for positions of river mouths), which provide total freshwater discharges of about 252, 137, 83, an 36 m^3 s^{-1} to the lake system in May, June, July and August of 1974 respectively (Table 1). Each river in the model is approximated by one grid cell wide (~500 m) and five grids long (~2 km) in the top z-level. The model salinity (S^h) at the head of each river is specified as

$$S^h = \frac{S^m \cdot V_c + S^r \cdot V_r}{V_c + V_r} \tag{4}$$

where S^m is the model salinity at the head of the river at previous time step; S^r is the salinity of river waters at the head, which is set to 0.4 psu; V_c is the volume of the model cell at the head of the river; and V_r is the volume of freshwater discharge from the river during one time step. The surface elevation at the head of the river (η^h) is given

$$\eta^h = \eta^m + V_r / S_c \tag{5}$$

where η^m is the model-calculated surface elevation at the head of the river at the previous time step, and S_c is the surface area of the model cell at the head of the river. The above specification of the salinity and surface elevation at the river head allows the buoyant estuarine waters to flow freely into the BdOL via the estuary with the model salinity at the river head (and mouth) varying according to the strength of the river discharge.

2.3 Model initial conditions

Due to unavailability of hydrographic climatology for the BdOL, we initialize the model temperature and salinity fields in baroclinic numerical experiments presented in Section 3 based on hydrographic measurements made in May 1974. (Hydrographic measurements made in July 1974 are used to validate the model results presented in Section 3.2). Fig. 3 presents vertical profiles of observed temperatures and salinities made on May 22 and 23, 1974, in the BdOL. The reader is referred to Gurbutt and Petrie (1995) for description of measurements and positions of hydrographic stations during this 2-day period. The temperature and salinity measurements made over the northern BdOL have similar vertical profiles at different stations, which can be characterized as a three-layer structure in the vertical with a relatively warm (~6 to 8℃) and fresh (~20 to 21 psu) in the top 5 m; relatively cold (~0.5℃) and salty (~25 to 26 psu) below 30 m; and a strong thermocline from about 5 m to 30 m. Except for a few profiles, the vertical profiles of observed temperatures and salinities also have similar vertical structures at different stations over the southern BdOL. Due

to the restriction of the Barra Strait, however, the observed salinities in the southern BdOL are relatively fresher (~20 to 22 psu) and vertically more uniform than those in the northern BdOL. The observed temperatures in the southern BdOL are relatively colder in the top 10 m, and relatively warmer below 10 m, than those in the northern BdOL.

For simplicity, we set the model initial temperature and salinity (on May 23, 1974) to be vertically stratified and horizontally uniform in the northern and southern parts of the BdOL as separated by the Barra Strait. The vertical stratifications of initial model temperatures and salinities over each part of the BdOL are the same as those averaged from the observed hydrographic measurements. Along the Barra Strait the initial model temperature and salinity are the linear combination of averaged profiles in basins on both side of the Strait. The initial model currents are set to zero (i.e., cold start).

3 Model results

3.1 Process study of lake responses to tides, wind forcing, and river runoff

(a) Barotropic response to M_2 tide

We first run the 3D circulation model in barotropic mode (with the model temperature and salinity set to be constant in time and space) forced by the semi-diurnal (M_2) tidal surface elevation specified at Table Head Point at the northern open boundary (Exp-M2, Table 2) to examine the barotropic M_2 tidal circulation in the BdOL. The amplitude of the semi-diurnal tidal elevation at the Point is set to 0.342 m based on the estimation made by Petrie (1999). We integrate the model for 22 days and the model results of the last 20 days are used to examine the tidal circulation and associated residual flows.

The currents produced by the tidally-forced model in Exp-M2 (Figs. 4-6) are characterized by intense jet-like tidal flows in the GBC and Barra Strait and relatively weak currents in the other regions of the BdOL. The general tidal circulation pattern produced by the model agrees qualitatively with previous findings based on current-meter observations (Krauel 1975a, Petrie 1999) and numerical results produced by the 2D finite-element numerical model (Dupont et al. 2003). At the high tide stage (in terms of sea levels at Table Head Point along the northern open boundary), the intense jet-like tidal flow in the GBC runs inward (southwestward) from the mouth to the south end of the Channel, with a maximum speed of about 80 cm s^{-1} near Seal Island (at about 13 km from the mouth of the channel) (Fig. 4a). After emanating from the GBC, the tidal flow separates into two main branches, with one branch veering westward and entering St. Patrick's Channel, and the

other branch spreading gradually over the northern region of the North Basin. As the tide falls through zero sea level (Fig. 4b), the along-transect currents have a similar circulation pattern as at the high tide stage but with weaker amplitudes. There are still large inward surface currents in the GBC, Barra Strait and adjacent areas at this stage (Fig. 4b), with a maximum speed of about 70 cm s^{-1}. At the low tide stage (Fig. 4c), the northwestward surface currents in the North Basin and northeastward currents in St. Patrick's Channel merge over the south end of the GBC and form an intense jet-like flow that runs seaward along GBC, with a maximum speed of about 70 cm s^{-1}. The along-transect flow runs northeastward, with relatively strong currents near Seal Island and at the mouth of the GBC (Fig 4c). At the same stage, there is also a relatively strong northeast flow in the Barra Strait and adjacent areas (Fig. 4c). The intense jet-like flow continues to flow northeastward in the Barra Strait as the tide rises, with a maximum speed of about 60 cm s^{-1} at the rising tidal stage (Fig. 4d).

Below the surface layer, the along-transect tidal flows vary significantly with depth. Figure 5 shows vertical distributions of horizontal (i.e., along-transect) and vertical components of tidal flows interpolated from model results along the longitudinal axis of the GBC marked in Fig. 1 at four different tidal stages. At the high tide stage (Fig. 5a) and the low tide (Fig. 5c), the tidal flows along this transect reach a maximum speed in the top 20 m near Seal Island. The amplitudes of tidal currents decrease with depth at all 4 tidal stages. The significant horizontal and vertical variations of the inward (Figs. 5a,b) and seaward (Figs. 5c,d) currents along this transect are mainly due to changes in the water depths and shape in the Channel.

The tidal flow through the Barra Strait also has significant vertical shears. Fig. 6 shows the vertical distributions of the horizontal and vertical components of the tidal currents along a northeast-southwest transect passing through the Barra Strait at four different tidal stages defined in terms of the model-calculated surface elevations at Iona. It should be noted that the semi-diurnal tide at Iona lags about 3 hours behind that at Table Head Point, and the four tidal stages in Figs. 5 and 6 occur at different times. At the high tide stage (Fig. 6a) the along-channel flow is southwestward and relatively strong in the Strait. This along-channel flow continues to flow southwestward in the top 20 m over the southern transect, with a maximum speed of 40 cm s^{-1}. The vertical currents are relatively weak and mainly upward on the northern transect. Over the southern part of the transect, the vertical currents are relatively strong and downward in the top 20 m, and relatively weak and upward in the bottom few meters. At the falling tide stage (Fig. 6b) and low tide stage (Fig. 6c), the along-transect currents in the Strait flow northeastward, with strong currents over the central part and relatively weak over the two ends of the Strait. At the rising tide stage (Fig. 6d), the southern

North Basin water flows southwestward and forms the intense inward jet-like flow over the Strait. Upwelling and downwelling occur, respectively, on the north and south ends of the Strait.

To assess the model performance in simulating the semi-diurnal tides in the BdOL, we compare the model-calculated surface elevations with the surface elevation measurements made at 9 tide gauges in the BdOL in 1973 and 1974 by Krauel (1975a, 1975b). Petrie (1999) estimated the amplitudes and phases of the M_2 tidal sea levels from Krauel's sea level observations. The observed amplitudes of the M_2 surface elevations decrease dramatically in the GBC, from 34.2 cm outside the mouth near Table Head, to about 3.7 cm at Baddeck, and then rise slightly as the tidal waves propagate inside the BdOL (Fig. 7a). The observed phases of the M_2 surface elevation in the northern part of the GBC have a tendency to lead the phase outside of the mouth (Fig. 7b). For example, the observed M_2 phase at Seal Island leads that at Table Head Point by about 20.7 min (more discussion is given later). Outside of the southern GBC, the observed M_2 phase lags behind that at Table Head Point with a maximum phase lag of about 4 hours and 29.1 minutes in the Bras d'Or Lake.

We compute the amplitudes and phases of the M_2 tidal surface elevations at 9 tide gauge stations from the model results in Exp-M2 and compare them with amplitudes and phases estimated from the observations by Petrie (Fig. 7). The model-calculated M_2 tidal surface elevations agree reasonably well with the observations, except for those at Black Rock and Duffus Point over the northern GBC. Our model results exhibit a ~75% reduction of surface elevation and a phase advance of ~24 minutes at Seal Island relative to Table Head Point, which agrees remarkably well with the observed deduction of tidal amplitude of ~79% (Fig. 7a) and phase advance of ~21 minutes (Fig. 7b). The model results underestimate the observed amplitude of M_2 surface elevation at Black Rock and overestimate at Duffus Point (Figure 7a). It is interesting to note that, although the surface elevation specified at Table Head Point is symmetric, the calculated surface elevation at Seal Island has a large ebb-flood asymmetry, with a relatively longer duration during the flood tide and shorter duration during the ebb tide (Fig. 8).

To examine the role of the nonlinear tidal dynamics in generating the ebb-flood asymmetry in the GBC, we conduct the second numerical experiment (Exp-M2-L, Table 2) using a linear tidal circulation model by eliminating the nonlinear terms in the model momentum equations and using the linear bottom friction parameterization, with the linear bottom friction coefficient set to 0.01 cm s^{-1}. The linear model is forced by the same tidal forcing, with the same model parameters as in Exp-M2. The surface elevation produced by the linear model is symmetric at Seal Island, with an amplitude deduction of ~61% relative to Table Head Point, which differs significantly from the results produced by the fully nonlinear model in Exp-M2 (Fig. 8). Furthermore, the tidal phase at

Seal Island produced by the linear model lags behind that at Table Head Point, with a phase lag of ~21 minutes.

A logical question is raised as to whether the nonlinear advection terms in the momentum equations or the nonlinear bottom friction plays the dominant role in generating the ebb-flood asymmetry in the GBC. To address this issue we conduct two additional numerical experiments. The circulation model in Exp-M2-LM (Table 2) uses the nonlinear bottom friction parameterization but excludes the nonlinear advection terms, and the model in Exp-M2-LB uses the linear bottom friction parameterization with the nonlinear advection terms. The model-calculated surface elevations in Exp-M2-LM are very similar to those produced by the nonlinear model in Exp-M2, while the model-calculated surface elevations in Exp-M2-LB are very similar to those produced by the fully linear model in Exp-M2-L, indicating that the nonlinear bottom friction parameterization plays a dominant role in generating the nonlinear characteristics (i.e., the asymmetry of the tidal surface and the tidal phase advance) at Seal Island. Our model results also support the argument made by Petrie (1999) that the phase difference is caused primarily by the strong frictional effects in the northern part of the Channel.

To determine the role of the nonlinear terms in the continuity equation, we conduct an additional numerical experiment using nonlinear advection terms and nonlinear bottom friction parameterization in the momentum equations but excluding nonlinear terms in the continuity equation. The calculated M_2 tidal amplitude and phase lag at Seal Island are the same as those produced by Exp-M2, except the zero time mean sea level while Exp-M2 generates a positive time mean sea level of ~2 cm. This means that the nonlinear terms in the continuity equation only affect the time mean sea level and don't play a role in generating the asymmetry of the tidal surface and the tidal phase advance at Seal Island.

The nonlinear interaction of the tidal currents with the local bathymetry generates tidal residual flow. We compute tidally averaged near-surface residual flow (Fig. 9) from the model results in Exp-M2 during the last two M_2 tidal cycles. Large tidal residual currents occur only in the GBC, Barr Strait and their vicinities, with a maximum speed of greater than 20 cm s^{-1} in GBC (not shown). The model-calculated near-surface residual flow is characterized by a large-scale cyclonic gyre over the northern North Basin, and two anticyclonic recirculation gyres over areas respectively to the north and south of the Barra Strait (Fig. 10), with a typical speed of 10 cm s^{-1}. The residual currents estimated by this coarse-grid model are rather small over other areas of the BdOL.

(b) Barotropic response to wind forcing

To examine the dynamic response to wind forcing in the BdOL, we integrate the fully non-linear circulation model in barotropic mode for 10 days from a state of rest with suddenly imposed horizontally uniform northeastward wind of 0.144 N m^{-2} (i.e., a wind speed of 10 m s^{-1}) (Exp-W, Table 2). Tidal forcing is excluded in this experiment.

Figure 10 presents time series of eastward and northward components of wind-driven currents at sites C3, C5 and C6 marked in Fig. 1. The model-calculated near-surface currents at the three sites accelerate downwind in the first few hours (Csanady 1982). After experiencing significant fluctuations associated with the propagation and dissipation of barotropic waves generated by the suddenly imposed wind forcing, the model-calculated currents reach a quasi-steady state after 2 days (Fig. 10), with near-surface currents of about 10 cm s^{-1} and roughly southeastward at C3 in the central North Basin, about 9 cm s^{-1} and roughly northeastward at C5 in the Barra Strait, and about 25 cm s^{-1} and roughly eastward at C6 in the northern part of Bras d'Or Lake.

The model-calculated surface elevations at day 10 have spatial variations of about 8 cm in response to the steady wind forcing in the BdOL (Fig. 11a). It should be noted that the surface elevations shown in the figure are relative to the zero surface elevations at the northern open boundary. The model generates the wind-driven setdown of about 2 cm in East Bay, Bras d'Or Lake and in the northeastern part of St. Andrew's Channel, and wind-driven setdown of about 10 cm in St. Patrick's Channel and about 6 cm in West Bay.

The near-surface (2 m) circulation produced by the model in Exp-W is characterized by two relatively strong coastal jets in the southern BdOL with a maximum speed of more than 30 cm s^{-1} (Fig. 11a). A strong and broad jet flows along the northwestern coast of West Bay and veers eastward over the northern part of Bras d'Or Lake, while the other, relatively weaker and narrower jet runs along the southern coast of West Bay and continues to flow eastward, reaching the eastern coast of East Bay. Divergences and convergences occur, respectively, over the southwestern portion of West Bay and northeastern portion of East Bay, which must be balanced by sub-surface southwestward flows over these regions. There are also narrow jets flowing northeastward along the eastern and western coasts of St. Andrew's Channel, between which there are roughly eastward currents due to the Ekman effect.

The sub-surface (15 m) circulation produced by the model in Exp-W is characterized by a nearly southwestward sub-surface flow running from central East Bay, through the central region of Bras d'Or Lake and finishing in West Bay (Fig. 11b), with a maximum of 15 cm s^{-1}. This southwestward flow in the deep waters of West and East Bays connects the near-surface northeastward outflow in

the region through upwelling over southwestern West Bay and downwelling over northeastern East Bay.

(c) Baroclinic response to river runoff

We next run the lake circulation model in baroclinic mode forced by freshwater discharges from 17 rivers in the BdOL (Exp-R, Table 2). We initialize the model with spatially uniform but vertically stratified temperature and salinity over the northern and southern BdOL respectively as described in Section 2.2(d) and integrate the model for 30 days. The discharge rates of freshwater from 17 rivers are based on the monthly mean values in May 1974. All other model forcing, including tidal and sub-tidal forcing at the northern open boundary, surface net heat flux, and surface wind forcing, are excluded in this experiment.

The near-surface (2 m) salinities at day 30 in Exp-R (Fig. 12a) are characterized by relatively low values near the mouths of 17 rivers and over Whycocomagh Bay, Denys Basin, and St. Patrick's Channel; high values over the northern GBC; and spatially uniform (~20.5 psu) in other areas of the BdOL. The low near-surface salinities of less than 18 psu in Patrick's Channel are associated with large amounts of freshwater discharges from the two largest rivers in the BdOL, the Middle and Baddeck Rivers, of which the catchment areas account for 25% of the total watershed area. The low salinities in Whycocomagh Bay and Denys Basin are associated with the combination of large freshwater inputs in the two areas and restricted connection between these isolated bays and main basins of the BdOL. The high near-surface salinities over the northern GBC indicate the influence of the high salinity waters over Sydney Bight. The model-calculated sub-surface (9 m) salinities are characterized by relatively low values over the southern part of the BdOL and the high values over GBC and St. Andrew's Channel. This pattern is associated with the restricted transport of the Barra Strait.

The model-calculated near-surface currents in Exp-R have relatively strong northeastward outflow of about 5 cm s^{-1} in St. Patrick's Channel, southwestward outflow of about 2 cm s^{-1} in East Bay, and northeastward outflow in West Bay. The latter two outflows form a cyclonic gyre over central Bras d'Or Lake, with a typical speed of about 5 cm s^{-1}. After emanating from the St. Patrick Channel, the northeastward outflow separates into two main branches, with one branch veering cyclonically to flow into the GBC and forming a strong seaward jet of about 5 to 10 cm s^{-1} in the Channel, and the other branch turning anticyclonically and spreading gradually into the northern North Basin.

The sub-surface (9 m) currents in Exp-R are characterized by strong inward flow through the GBC, the northward flow and the westward flow over the northern North Basin which merge over the

south end of the GBC and form an intense upstream flow that runs westward along St. Patrick's Channel (Fig. 12b). In the southern BdOL, there is a relatively weak cyclonic gyre located in the central region of the Bras d'Or Lake. There are also relatively large sub-surface currents near the river mouths due to large density gradients associated with freshwater runoff.

The large-scale features of the buoyancy-driven circulation produced by the model in Exp-R are consistent qualitatively with previous knowledge of general circulation associated with river runoff in the BdOL based on the observations and box model results discussed in Gurbutt and Perie (1995). They suggested that the surface waters of the BdOL flow from West and East Bays and join with the outflows from St. Patrick's Channel to form an intense near-surface seaward current through the GBC that discharges into Sydney Bight, and a sub-surface flow roughly in the opposite direction. The model results also generate a two-layer estuarine circulation pattern near river mouths and a cyclonic gyre over the central Bras d'Or Lake. This two-layer circulation pattern introduces significant mixing at the interface of the two layers and strong upwellings at the river mouths.

3.2 Reproducing circulation and hydrographic structure in June and July 1974

In this section, we use the nonlinear circulation model in baroclinic mode to reconstruct the 3D circulation and thermal structure in the BdOL in June and July 1974 (control run or Exp-C, see Table 2). The model is forced by the external forcing discussed in Section 2.2, which includes boundary forcing, wind stress, heat flux, and buoyancy forcing associated with freshwater runoff from 17 major rivers. The boundary forcing specified at the northern open boundary includes the sub-tidal sea level fluctuations and tidal surface elevations estimated from five tidal constituents made by Petrie (1999). The model uses the initial conditions discussed in Section 2.3, and is integrated from a state of rest for 58 days from May 23 to July 19, 1974.

We first assess the model performance by comparing the model results in Exp-C with the observed currents at C3, C5, C6 and C10 (see their positions marked in Fig. 1) made in June and July 1974, and temperature and salinity distributions in the BdOL derived from the CTD survey during 15-19 July, 1974. To measure the model errors, we calculate the misfit between the observed and model-calculated currents defined as:

$$\gamma^2 = Var(M\text{-}O)/Var(O) \tag{6}$$

where M and O represent respectively the model-calculated and observed currents, and Var represents the variance. Physically, the γ^2 value is the variance of the model errors normalized by

the observed variance. The smaller γ^2 is, the better the agreement between the model and observations.

Comparison of the observed and simulated currents at depths of 5 m and 10 m at site C5 in the Barra Strait (Fig. 13) is adjusted by multiplying the model results by a factor of 1.3 because the cross-sectional area of the Barra Strait in the model is ~1.3 times larger than the actual area estimated from the chart. The adjusted model results reproduce the observed currents at this site reasonably well, particularly the northward components of the observed currents, with γ^2 values in the range of 0.25 to 0.44, indicating that the model estimates reasonably well the water transport through the Strait.

The circulation model performs less well in reconstructing the observed currents at three other sites (Figs. 14 and 15). The model results significantly underestimate the observed currents at depths of 5 m and 20 m at site C3 in the central North Basin, with γ^2 values in the range of 0.99 to 1.34. It should be noted that the local bathymetry around site C3 varies by about 100 m within a horizontal distance of less than 300 m. The topography at this site is not well represented in the model due to the model horizontal resolution of about 500 m, which could partially explain the large discrepancy between modeled and observed results at this location.

The circulation model captures the typical amplitude of the observed currents at 5 m at C6 and at 15 m at C10 in Bras d'Or Lake (Fig. 15), with γ^2 values between 0.88 and 1.33. The tidal currents in Bras d'Or Lake are very weak and the temporal variability of sub-surface currents at the two sites are mainly associated with wind forcing and boundary currents associated with the air pressure changes discussed in Section 2.2. The model fails in reproducing the large observed currents during a 2-day period of day 176-178 (Figs. 15b,c), which is probably associated with the spatial variability in the local wind field, which was not considered in this study. It should be noted that the observed and simulated currents could still be correlated even if the γ^2 value is greater than 1. As an example, the correlation coefficient between the two time series shown in Fig. 15a is 0.35, which is statistically significant at the 99.999% confidence level, while the γ^2 value between the two time series is 1.33.

The observed surface temperature on 15-19 July 1974 along a transect extending from the mouth of the GBC to East Bay (Fig. 1, Gurbutt and Petrie 1995) exceeds 16^{o}C in East Bay and the GBC, and is ~15^{o}C in the Bras d'Or Lake and the North Basin. The sub-surface temperature is relatively cold, and about 1^{o}C centered at 100 m in the central North Basin, and ~2^{o}C centered at 50 m in central Bras d'Or Lake. The observed vertical distributions of temperature are vertically uniform in the

GBC and much warmer than those in other parts of the BdOL, due primarily to strong mixing in the GBC. The thermocline in the interior of the BdOL is located between 15 to 20 m depth. The surface salinity changes significantly from ~30 psu at the mouth of the GBC to ~21 psu in Bras d'Or Lake and East Bay, with a surface salinity front in the northern GBC. The salinity along the transect also changes significantly in the vertical in the GBC and North Basin, with a halocline at the depth of about 15 m. The salinity is relatively uniform below 30 m in North Basin with a value of ~25 psu. Due to the limited exchange of the Barra Strait connecting the two main parts of the BdOL, the salinity in the southern BdOL is lower than that in the northern part at the same depths (Fig. 16).

The model-calculated temperature and salinity distributions averaged during the same period of July 15-19, 1974 along the same transect are shown in Fig. 17. The model reproduces the general features of the observed hydrographic distributions along the transect, with relatively warm and fresh surface waters overlying relatively colder and saltier sub-surface waters over North Basin, Bras d'Or Lake and East Bay, and vertically uniform temperatures and highly stratified salinities in the GBC. Large differences occur, however, between the simulated and observed hydrographic distributions along the transect (Figs. 16 and 17). The model underestimates the near-surface temperature, with a maximum of ~16^{o}C in northeastern East Bay and ~15^{o}C in GBC, and overestimates the temperature in the deep regions, with a minimum of less than 2^{o}C below 50 m in the central North Basin, and of ~4^{o}C below 50 m in central Bras d'Or Lake. The thermocline produced by the model in Exp-C is at about 15 to 30 m, which is deeper and more diffuse than the observed structure.

The plausible reason for the model deficiency in simulating the near-surface temperatures during the study period is due to the estimation of surface insolation using climatological fields. The model deficiency in simulating the deep water temperature is due probably to the maximum depth of 200 m set in the model which prevents the deep waters in St. Andrew's Channel from exchanging with the deeper and colder waters below 200 m.

The model reproduces well the observed surface salinity front in the northern GBC and the low salinity in the Southern part of the BdOL, with a minimum of 20 psu (Fig. 17b). In the North Basin, the halocline produced by the model is deeper and more diffuse compared with the observations. The model also underestimates the observed salinity stratification in the GBC, for which the exact reason is unknown, and could partially be associated with the coarse model horizontal resolution used in this study.

A detailed analysis of instantaneous near-surface currents and salinity produced by the model in Exp-C from 15-19 July, 1974 (day 198.2 to 198.5; see Fig. 18) reveals the strengths and weaknesses of the model in simulating the real hydrodynamics of this complex water body. During this summer period, the local wind stresses are consistently towards the northeast (i.e. SW winds), but are relatively weak at days 198.2 and 198.3 and relatively stronger at days 198.4 and 198.5. The near-surface currents at day 198.2 are characterized by an intense seaward (northeastward) jet in the GBC with a typical speed of 20 to 30 cm s^{-1}, a northeastward outflow in St. Patrick's Channel of about 5 cm s^{-1}, and relatively strong and northeastward currents over southeastern North Basin of about 10 cm s^{-1} (Fig. 18a). In Bras d'Or Lake the near-surface currents are approximately southward or southeastward, flowing into the southern part of the Lake.

Different physical processes are responsible for the above-mentioned currents in the BdOL. The intense jet in the GBC at day 198.2 is mainly associated with the seaward tidal circulation in the channel. The outflow in St. Patrick's Channel is produced mainly by the buoyancy forcing associated with large freshwater runoff from the Middle and Baddeck Rivers. The northeastward currents over North Basin are a combination of the tidal flow and density-driven currents in the region at this time. The near-surface circulation in Bras d'Or Lake at day 198.2 is mainly associated with the pressure gradients generated by wind forcing in the recent past.

At day 198.3, the near-surface currents in the GBC are intense and inward due to the strong tidal flow in the Channel, with significant spatial variations of about 100 cm s^{-1} near Duffus Point and about 10 cm s^{-1} near the south end of the Channel (Fig. 18b). Emanating from the southern end of the GBC, the tidal flow enters the northern part of North Basin and veers cyclonically to flow into St. Andrew's Channel. Associated with the tidal circulation in the BdOL, there is an intense southward flow through the Barra Strait at this time. The near-surface currents in St. Patrick's Channel and Bras d'Or Lake at day 198.3 are relatively weak and have large spatial variability.

The wind stress is ~0.06 N m^{-2} and approximately northeastward at day 198.4. The near-surface currents in the GBC remain inward, but much weaker than those at day 198.3 (Fig. 18c). Due to the combination of the wind forcing and buoyancy forcing associated with river runoff, there is a strong northeastward outflow in St. Patrick's Channel, which merges with the southwestward tidal flow emanating from the south end of the GBC to form strong southeastward currents over the northern section of the North Basin. The near-surface currents in St. Andrew's Channel are approximately eastward in response to the northeastward wind forcing. The near-surface currents in Bras d'Or Lake at day 198.4 are roughly eastward and spatially uniform at ~8 cm s^{-1}, which is also forced mainly by the wind.

At day 198.5, the near-surface currents in Bras d'Or Lake, North Basin, and St. Andrew's Channel are generally stronger than those at the other three times, forced mainly by the strong northeastward wind stress of ~0.11 N m^{-2}. The strong northeastward outflow in St. Patrick's Channel is due to the combination of buoyancy and wind forcing. The intense seaward (northeastward) jet-like flow in the GBC at day 198.5 is associated mainly with the tidal circulation in the Channel.

The model-calculated near-surface (2 m) salinities at day 198.2 in Exp-C (Fig. 18a) are characterized by relatively low values (< 18 psu) in Whycocomagh Bay, Denys Basin, and St. Patrick's Channel, high values (> 24 psu) in the northern section of the GBC, and spatially uniform values of about 21 psu in other areas of the BdOL. The near-surface salinity distributions at the other three times shown in Figs. 18b-c have similar patterns at day 198.2, except that salinity fronts over the northern GBC move back and forth, advected by strong tidal currents in the Channel. The freshwater plume over the northern North Basin spreads and shrinks associated with the near-surface currents. For example, the isohaline of 21 psu over the North Basin is roughly along the northeast-southwest axis of the basin at day 198.2, while it almost reaches the southeast coastline of the Basin at day 198.5 associated with the freshwater plumes spreading under the eastward currents.

To determine the contribution of the density-driven flow to the 3D circulation in the BdOL, we follow Xing and Davies (2001) and run the circulation model (Exp-D, Table 2) by initializing the model with the temperature and salinity fields produced by the model in Exp-C on July 19, 1974. Other model external forcing, such as the tidal and sub-tidal sea level variation, wind stress, heat flux, and freshwater runoff, are all excluded. The model is integrated in prognostic mode from a state of rest and run for 3 days to reach a quasi-steady state.

The near-surface (2 m) salinity produced by the model in Exp-D (Fig. 19a) has a similar pattern to that in Exp-R (Fig. 12a), with relatively low values over Whycocomagh Bay, Denys Basin, and St. Patrick's Channel, high values over the northern GBC, and spatially uniform values of ~21 psu in other areas of the BdOL. Over several river mouths, the model-calculated salinities in Exp-D are slightly higher than those in Exp-R, due mainly to weaker stratifications and zero fresh water runoff from rivers in Exp-D than those in Exp-R. The model-calculated near-surface currents (2 m, Fig. 19a) have a similar pattern to those in Exp-R (Fig. 12a). However, the cyclonic gyre in the southern BdOL is relatively smaller but stronger compared to that in Exp-R in both the 2m and 9m depth layers (Fig. 19a, b). The sub-surface currents (9m, Fig. 19b) over St. Patrick's Channel, GBC and Barra Strait are in the opposite directions to the flow in the upper layer. The sub-surface currents in the southern BdOL show a similar pattern to the near-surface currents but with weaker amplitudes.

The vertical distribution of modeled currents and salinity (Exp-D) reveals the estuarine circulation in both the GBC and Barra Strait (Figs. 20 and 21). The brackish surface water flows from the North Basin to the Atlantic Ocean with a maximum speed of more than 12 cm s^{-1}, while the salty sub-surface water flows from the Atlantic Ocean into the BdOL with a maximum speed of ~10 cm s^{-1}. The salinity changes significantly in the horizontal and vertical, with a salinity front in the entrance of the GBC (Fig. 20). A similar circulation pattern is presented in the Barra Strait with a maximum outward flow of 5 cm s^{-1} and an inward flow of the same magnitude (Fig. 21). A northeastward flowing tongue of brackish water extends from Bras d'Or Lake to North Basin in the top 5 m with a salinity of ~21 psu. These features of the density-driven currents in the BdOL demonstrate a typical 2-layer estuarine current pattern.

4 Sensitivity study

To investigate the influence of the sub-tidal sea level variations at Sydney Bight, we perform an additional experiment with the sub-tidal sea level variations excluded at the open boundary (Exp-S, Table 2). Other meteorological forcing is set to the same as the control experiment (Exp-C). This provides a direct comparison with the Exp-C, which was forced by both tidal and sub-tidal sea level variations at the model open boundary. Figure 22 compares the depth-mean residual currents (after tidal currents have been removed and a 25-hour low-pass filter is applied to eliminate any additional tidal components) along the channel axis for the Barra Strait produced by the model in Exp-C and Exp-S with the observations. The γ^2 values calculated using (6) for Fig. 22a and b are 0.38 and 0.81 respectively, which indicates that the model results in Exp-C reproduce the observations better than those in Exp-S.

5 Summary and discussion

Simulating the three-dimensional (3D) circulation in topographically complex ecosystems experiencing multiple forcing across the water-water, air-water and land-water boundaries poses a severe challenge to both physical oceanographers and computational mathematicians (Csanday 1982). Yet, it is in just such waters near the coasts that there exists the most urgent need for accurate and high-resolution models due to intense interactions between terrestrial humans and the ocean realm. The 3D hydrodynamic model presented in this study is the most detailed and accurate model to date for the Bras d'Or Lakes estuary in terms of its temporal and spatial resolution and its incorporation of multiple external forcings. Our purpose is to refine and adapt this model to critical management applications in a charismatic estuarine ecosystem. Before this can occur, however, the model must be evaluated and refined to a stage where it has sufficient skill to meet the needs for

prediction of the structure and dynamics of water flow and density. This study is the first step in developing such skill for the Bras d'Or model.

The circulation model adapted to the Bras d'Or ecosystem is based on the 3D, finite-difference, z-level circulation model known as CANDIE (Sheng et al. 1998). As with all such numerical models, it is challenged by irregular boundaries and complex topography, and excels at resolving density fields and computational efficiency. The micro-tidal regime of the Bras d'Or Lakes minimizes the extent of dry/wet boundaries, however, and the capacity of the CANDIE to be two-way nested (Sheng et al. 2005; Sheng et al., 2007) permits the resolution of very complex shorelines and bathymetries within a coarser grid model. Because the main demands of the Bras d'Or model will be the simulation of trajectories of dissolved and particulate materials through Eularian-Lagrangian transforms and bio-physical tracking (i.e. connectivity studies, e.g. Tang et al. 2006), and the prediction of nearshore temperature and salinity variability that controls oyster growth and MSX infectivity (Burreson and Ford 2004), we conclude that the fully 3-D finite difference model presented here is a suitable tool for the jobs.

In the first instance, the 3D circulation model was used for a process study of 3D circulation to ascertain the relative and absolute contributions of the three major types of physical forcing known to be important in enclosed seas: tidal forcing across the northern open boundary and through topographically complex channels, wind forcing in a topographically complex terrain where local steering and circulations occurs at spatial scales equal to or smaller than the model domain, and buoyancy forcing associated with localized heat fluxes and very significant inputs of freshwater runoff from the large, complex watershed of the Bras d'Or ecosystem. The progressive series of nine experiments presented in this study allowed us to tease apart the effects of different forcing, as well as to evaluate the effects of various parameterizations reflecting the simplifying assumptions of the model. The results of the process analysis demonstrate that the three main forcing components contribute approximately equally to hydrodynamic circulation in the Bras d'Or Lakes, with each having a domain of dominance. Running the model with each forcing term individually, and then with them all together allows us to rank their respective contributions to the hydrodynamics of the Bras d'Or ecosystem, and to detail the circulations associated with each.

The M_2 tidal circulation produced by the model is characterized by an intense tidal jet with large changes in amplitudes and phases of the M_2 surface elevations in the Great Bras d'Or Channel, a strong jet through the Barra Strait, and weak tidal currents with small M_2 surface elevations in other areas of the BdOL. Two significant eddies of the tidal residual circulation are generated at the entrances to the narrow channel (i.e., the Barra Strait) linking the two main basins of the estuary.

The model results reproduce reasonably well the observed tidal amplitudes and phases at 9 tide gauge stations in the BdOL, giving us confidence that the model captures the critical effects of tidal forcing well. Examination of the nonlinear tidal dynamics demonstrates that the nonlinear bottom friction term plays a dominant role in generating the phase advance in the entrance of GBC, which is consistent with previous studies (Petrie 1999, Petrie and Bugden 2002).

The model-calculated near-surface circulation in response to a steady 10 m s^{-1} northeastward wind has a strong and broad northeastward jet along the western coast of Bras d'Or Lake and two relatively weak and narrow northeastward jets along the East coasts of Bras d'Or Lake and St. Andrew's Channel.

The baroclinic response to freshwater discharges from 17 major rivers in the BdOL is characterized by a typical 2-layer estuarine circulation, with outflows in the upper layer from St. Patrick's Channel, West Bay and East Bay. An intense seaward jet runs through the Great Bras d'Or Channel and discharges into Sydney Bight. The circulation pattern in the lower layers is very similar to that in the upper layer, except the flow directions are in opposite directions. A large gyre in the largest basin (Bras d'Or Lake) is forced by density-driven currents, and may be of ecological significance. The model's ability to portray the time-evolving temperature-salinity field at the scales of individual channels, bays and lagoons, even in very shallow water, is impressive.

Validation of model results by direct comparison with the only suitably detailed oceanographic data for the ecosystem provided us with a clear evaluation of the model's shortcomings, thereby identifying paths to improvement. We were able to reconstruct the 3D circulation and hydrographic distributions in the summer months of 1974 by driving the 3D circulation model with realistic boundary forcing, time-varying wind forcing, surface heat flux, and freshwater inputs from the 17 major rivers. The model boundary forcing includes tidal surface elevations calculated from five principal tidal constituents and sub-tidal sea level changes at the mouth of the Great Bras d'Or Channel. The model results agree qualitatively with the observed currents and hydrographic distributions in the BdOL during this period, and demonstrate the importance of the sub-tidal variations in sea level at the mouth of the GBC to the circulation interior of the BdOL. The model significantly underestimates measured water current speeds (but not directions) in virtually all locations and conditions and also underestimates the density stratification.

The reasons for the model's inaccuracies are manifold, but coarse spatial resolution relative to the characteristic length scales of topographic and shoreline features in the Bras d'Or, and forcing functions that are too coarsely averaged in space or time are the main problems identified by our

analysis, rather than inherent limitations of the equations or computational algorithms. The presence of several narrow channels between basins (e.g. Little Narrows, Fig. 1) and restricted passages in the BdOL (including those with connections to the open ocean, e.g. Little Bras d'Or Channel and St. Peter's Canal, Fig. 1) that are of comparable or even smaller widths than the model's horizontal resolution (~500 m) poses a severe challenge to the model's ability to capture many detailed circulation features, even though the volume transport and associated temporal variability through the channels was depicted reasonably well. In order to resolve detailed circulation features within some key passages such as the Barra Strait and Little Narrows, a nested-grid circulation modeling system such as those used by Tang et al. (2006) and Sheng et al. (2006) is required. The other future improvements also include more realistic sea surface flux boundary conditions both in space and time.

6 Acknowledgements

The authors wish to thank Li Zhai for implementing the modified KPP scheme, and Gary Bugden, Jun Zhao, Liang Wang, and two anonymous reviewers for their useful comments and suggestions. This study was supported by Canada's Research Network in Aquaculture. JS is also supported by the NSERC/MARTEC/MSC Industrial Research Chair, and BH by a CBU/CFI Research Chair.

References

Burreson EM, Ford SE (2004) A review of recent information on the Haplosporidia, with special reference to *Haplosporidium nelsoni* (MSX disease). Aquat Living Resour 17:499-517

Csanady GT (1982) Circulation in the coastal ocean. Reidel Publishing Company, Dordrecht, Holland, 279 pp

Davidson F, Greatbatch RJ, deYoung B (2001) Asymmetry in the response of a stratified coastal embayment to wind forcing. J Geophys Res 106:7001-7016

Devies AM, Flather RA (1978) Computing extreme meteorologically induced currents, with application to the Northwest European continental shelf. Cont Shelf Res 7:643-683

Dupont F, Petrie B, Chaffey J (2003) Modelling the Bras d'Or BdOL. Can Tech Rep Ocean Sci 999: viii + 53 pp

Durski SM, Glenn SM, Haidvogel DB (2004) Vertical mixing schemes in the coastal ocean: Comparison of the level 2.5 Mellor-Yamada scheme with an enhanced version of the K profile parameterization. J Geophys Res 109(C01015). doi:10.1029/2002JC001702, 1-23

Geshelin Y, Sheng J, Greatbatch RJ (1999) Monthly mean climatologies of temperature and salinity in the Western North Atlantic. Can Tech Rep Hydrogr Ocean Sci 153: vi + 62 pp

Gill AE (1982) Atmosphere-Ocean Dynamics. Academic Press, San Diego, California, U.S, 33-36

Greenberg DA, Shore JA, Page FH, Dowd M (2005) A finite element circulation model for embayments with drying intertidal areas and its application to the Quoddy region of the Bay of Fundy. Ocean Modelling 10:211-231

Gurbutt PA, Petrie B (1995) Circulation in the Bras d'Or BdOL. Estuar. Coastal and Shelf Sci 41:611-630

Johnson S (2004) The Bras d'Or BdOL Watershed. Oceans and Coastal Management Division, Fisheries & Oceans Canada, Maritimes Region, Dartmouth, NS, Map 1pp

Krauel DP (1975a) The physical oceanography of the Bras d'Or BdOL 1972-1974. Bedford Institute of Oceanography, Fisheries and Marine Science Tech Rep, No. 570, 357pp

Krauel DP (1975b) A summary of the physical oceanography of the Bras d'Or Lake system. In the preceedings of the Bras d'Or BdOL aquaculture conference (McKay, G., ed.). College of Cape Breton press, Sydney, Canada, 29-43

Lambert TC (2002) Overview of the ecology of the Bras d'Or BdOL with emphasis on the fish. Proc N S Inst Sci 42:65-99

Large WG, Pond S (1981) Open ocean momentum flux measurements in moderate to strong winds. J Phys Oceanogr 11:324-336

Large WG, McWilliams JC, Doney SC (1994) Oceanic vertical mixing: a review and a modle with a model with a nonlocal boundary layer parameterization, Review of Geophysics, 32: 363-403.

Lu Y, Thompson KR, Wright DG (2001) Tidal currents and mixing in the Gulf of St. Lawrence: An application of the incremental approach to data assimilation. Can J Fish Aquat Sci 58:723-735

Mellor GL, Yamada T (1982) Development of a turbulence closure model for geophysical fluid problems. Review of Geophysical and Space Physics 20:851-875

Orlanski I (1976) A simple boundary condition for unbounded hyperbolic flows. J Comput Phys 21:251-269

Petrie B (1999) Sea level variability in the Bras d'Or BdOL. Atmos-Ocean 37:221-239

Petrie B, Bugden G (2002) The physical oceanography of the Bras d'Or BdOL. Proc N S Inst Sci 42:9-36

Sheng J, Wright DG, Greatbatch RJ, Dietrich DE (1998) CANDIE: A new version of the DieCAST ocean circulation model. J Atmos Oceanic Technol 15:1414-1432

Sheng J (2001) Dynamics of a buoyancy-driven coastal jet: The Gaspé Current. J Phys Oceanogr 31:3146-3163

Sheng J, Thompson KR, Cong L, Smith PC, Lawrence DL (2001) Effect of wind and local density on the subtidal circulation of the inner Scotian Shelf. Continental Shelf Res 21:1-19

Sheng J, Tang L (2003) A numerical study of circulation in the Western Caribbean Sea. J Phys Oceanogr 33:2049-2069

Sheng J, Wang L (2004) Numerical study of tidal circulation and nonlinear dynamics in Lunenburg Bay, Nova Scotia. J Geophys Res 109(C10018). doi: 10.1029/2004JC002404

Sheng J, Greatbatch RJ, Zhai X (2005) A new two-way nesting technique for ocean modeling based on the smoothed semi-prognostic method. Ocean Dynamics 55:162-177

Sheng J, Rao YR (2006) Circulation and thermal structure in Lake Huron and Georgian Bay: Application of a nested-grid hydrodynamic model. Cont Shelf Res 26: 1496-1518

Sheng J, Zhai X, Greatbatch RJ (2006) Numerical study of the storm-induced circulation on the Scotia shelf during Hurricane Juan using a nested-grid ocean model. Prog Oceanogr 70: 233-254

Sheng, J, Wang L, Andrefouet S, Hu C, Hatcher B, Muller-Karger FE, Kjerfve B, Heyman WD, Yang B (2007) Upper ocean response of the Mesoamerican Barrier Reef System to Hurricane Mitch and coastal freshwater inputs: A study using SeaWiFS ocean color data and a nested-grid ocean circulation model. J. Geophys. Res. (in press)

Smagorinsky J (1963) General circulation experiments with the primitive equation. I. The basic experiment. Monthly Weather Review 21:99-165

Stephenson M, McGladdery SE, Maillet M, Veniot A, Meyer G (2003) First reported occurrence of MSX in Atlantic Canada. J Shellfish Res 22:355

Stephenson M, Petrie B (2005) Oceanographic influences on the management of MSX disease of American oysters (*Crassostrea virginica*) in Atlantic Canada. Bull Aquacul Assoc Can 105:67-78

Tang L, Sheng J, Hatcher BG, Sale PF (2006) Numerical study of circulation, dispersion, and hydrodynamic connectivity of surface waters on the Belize shelf. J Geophys Res 111(C01003). doi: 10.1029/2005JC002930

Taylor RB, Shaw J (2002) Coastal character and coastal barrier evolution in the Bras d'Or Lakes, Nova Scotia. Proc N S Inst Sci 42:149-181

Water Survey of Canada (1972) Historical streamflow survey to 1970 – Atlantic Province. Inland Waters Directorate, Department of the Environment, Ottawa, Canada, 102pp

Xing J, Davies A (2001) A Three-dimensional Baroclinic Model of the Irish Sea: Formation of the Thermal Fronts and Associated Circulation. J Phys Oceanogr 31:94-114

List of Tables

List of Figures

Fig. 1 Map of the Bras d'Or Lakes region of Cape Breton Island, Nova Scotia, Canada, showing selected bathymetric features within the model domain (coloured shading and depths in metres), locations of sea level gauges (solid dots), hydrographic stations (pink triangles) and current meter stations (red triangles). Oceanographic transects through the Great Bras d'Or Channel, North Basin and Barra Strait, where current velocity is presented through the vertical, are marked by thick white lines. Hydrographic transects extending onwards through Bras d'Or Lake and into East Bay, where temperature-salinity data are presented through the vertical, are marked by red dashed lines. The rectangle marked by red solid lines shows the area chosen to present the model-calculated tidal residual flows (Fig. 9). Locations where the mouths of 17 rivers join the model boundary are marked with open red circles. The radius of each circle represents the ratio of freshwater discharge of the river to the total freshwater input to the lake system. Inset shows the location of North Sydney where the tide gauge data were collected, and the Sydney Airport where meteorological measurements were made

Fig. 2 Empirically measured forcing parameters used in driving a three-dimensional numerical circulation model of the Bras d'Or estuary. Time series of **a)** tidal forcing η_t, **b)** sub-tidal components of the observed sea levels (η_s) at North Sydney and sea level variations due to the inverse barometer effect (η_a) calculated from the air pressure measurements at Sydney Airport, and **c)** observed wind velocity at Sydney Airport during the study period from 00:00 May 23 (day 142) to 00:00 July 20 (day 200) in 1974

Fig. 3 Vertical profiles of **a)** observed temperatures and **b)** salinities in the Bara Strait separating the two great basins of the Bras d'Or estuary on May 22 and 23, 1974 (See Gurbutt and Petrie 1995 for the hydrographic locations)

Fig. 4 Near-surface (2 m) currents at four tidal stages in the Bras d'Or estuary (see Fig. 1), produced by the three-dimensional numerical circulation model in Exp-M2 (see Table 2). Current vectors are plotted at every third model grid. The model is forced by the M_2 tidal surface elevations specified at the northern open boundary. Insets show time series of sea levels at the northern open boundary, and the position in the tidal cycle is marked by the solid circle

Fig. 5 Distributions of horizontal (along transect) and vertical components of tidal currents along the longitudinal axis of the Great Bras d'Or Channel (Fig. 1), produced by a three-dimensional numerical model in Exp-M2 (Table 2). The distance in the plots is measured from the NE end

of transect. The model is forced by the M_2 tidal surface elevations specified at the northern open boundary. Insets show time series of sea levels at the northern open boundary, and the position in the tidal cycle is marked by the solid circle

Fig. 6 Distributions of horizontal (along transect) and vertical components of tidal currents along the longitudinal axis of the Barra Strait (Fig. 1), produced by the three-dimensional numerical model in Exp-M2 (Table 2) at four phases of the M_2 tide. The distance in the plots is measured from the NE end of transect. The model is forced by the M_2 tidal surface elevations specified at the northern open boundary of the Great Bars d'Or Channel. Insets show time series of sea levels at the Iona, and the position in the tidal cycle is marked by the solid circle

Fig. 7 Comparison of the observed (open circles) and model-calculated (solid triangles) **a)** amplitudes and **b)** phase lags relative to the tidal phase at Table Head Point of the M_2 surface elevations at 9 locations along a transect from the mouth of the Great Bras d'Or Channel to the NE end of West Bay, Bras d'Or estuary (Fig. 1). The model is forced by the M_2 tidal surface elevations specified at the northern open boundary of the Great Bars d'Or Channel. The thin dashed line in **b)** represents zero phase lag

Fig. 8 Time series of surface elevations specified for Table Head Point at the northern open boundary (solid line), and model-calculated surface elevations at Seal Island in Exp-M2 (dotted line) and Exp-M2-L (dashed line). The time mean value is removed from each of the time series. The three-dimensional numerical circulation model used for the two experiments is forced by the M_2 tide at the model's northern open boundary

Fig. 9 Near-surface tidal residual flow in the vicinity of the Barra Strait (Fig. 1), as calculated from the model results of Exp-M2 (Table 2). The three-dimensional numerical model is forced by the M_2 tidal elevation specified at the model's open boundary. Current vectors are plotted at every model grid

Fig. 10 Time series of **a)** eastward and **b)** northward components of the near-surface currents at locations C3, C5 and C6 along an oceanographic transect from the North Basin to Bras d'Or Lake (Fig. 1), produced by a circulation model in Exp-W (Table 2). The three-dimensional numerical model is forced only by the horizontally uniform and steady northeastward wind velocity of 10 m s^{-1}

Fig. 11 Model-calculated **a)** surface elevations and near-surface (2 m) currents, and **b)** sub-surface (15 m) currents at day 10 in a barotropic run (Exp-W) of a three-dimensional numerical circulation model of the Bras d'Or estuary (Fig. 1) forced only by steady northeastward winds of 10 m s^{-1}. Contour interval for elevations is 2 cm. Velocity vectors are plotted at every third model grid

Fig. 12 Model-calculated **a)** near-surface (2 m) currents and salinities, and **b)** sub-surface (9 m) currents and salinities at day 30 in a baroclinic run (Exp-R) of a three-dimensional numerical circulation model of the Bras d'Or estuary (Fig. 1) forced only by steady river runoff (Table 1). Velocity vectors are plotted at every third model grid

Fig. 13 Time series of scaled (x 1.3), model-predicted (blue plots) and observed (red plots) components of horizontal currents in depths of 5 m (**a** and **b**) and 10 m (**c** and **d**) at site C5 in the Barra Strait during the summer of 1974. The three-dimensional numerical model used for Exp-C (Table 2) was driven by all known forcing (i.e., tides, wind, buoyancy forcing and boundary flows associated with atmospheric pressure perturbations)

Fig. 14 Time series of model-predicted (blue plots) and observed (red plots) components of horizontal currents in depths of 5 m (**a** and **b**) and 20 m (**c** and **d**), at site C3 in the North Basin of the Bras d'Or estuary during the summer of 1974. The three-dimensional numerical model used for Exp-C (Table 2) was driven by all known forcing (i.e., tides, wind, buoyancy forcing and boundary flows associated with atmospheric pressure perturbations)

Fig. 15 Time series of model-predicted (blue plots) and observed (red plots) components of horizontal currents in depths of 5 m at site C6 (**a** and **b**) and 15 m at site C10 (**c** and **d**) in Bras d'Or Lake during the summer of 1974. The three-dimensional numerical model used for Exp-C (Table 2) was driven by all known forcing (i.e., tides, wind, buoyancy forcing and boundary flows associated with atmospheric pressure perturbations)

Fig. 16 Observed distributions of **a)** temperature and **b)** salinity along a transect from Table Head Point (left) to the head of East Bay (right) (see Fig. 1) during 15-19 July, 1974 made by Gurbutt and Petrie (1995). The bathymetry of the Great Bras d'Or Channel, North Basin, Barra Strait, Bras d'Or Lake and East Bay are located from left to right. The distance in the plots is measured from the north end of transect

Fig. 17 Model-calculated (Exp-C) time-mean distributions of **a)** temperature and **b)** salinity along a transect from Table Head Point (left) to the head of East Bay (right) predicted for 15-19 July,

1974. The bathymetry of the Great Bras d'Or Channel, North Basin, Barra Strait, Bras d'Or Lake and East Bay are located from left to right. The distance in the plots is measured from the north end of transect. The white areas reflect the coarseness of the model grid scale relative to the resolution of the bathymetry. The three-dimensional numerical model used to generate this plot in Exp-C (Table 2) was driven by all known forcing (i.e., tides, wind, buoyancy forcing and boundary flows associated with atmospheric pressure perturbations

Fig. 18 Model-calculated near-surface (2 m) currents and salinities in the Bras d'Or estuary at four different times during July, 1974. Velocity vectors are plotted at every third model grid. The three-dimensional numerical model used to generate this plot from Exp-C (Table 2) was driven by all known forcing (i.e., tides, wind, buoyancy forcing and boundary flows associated with atmospheric pressure perturbations)

Fig. 19 Model-calculated density-driven currents and salinities in the **a)** near-surface (2 m) layer and **b)** sub-surface (9 m) layer in the Bras d'Or estuary during July, 1974. Velocity vectors are plotted at every third model grid. The three-dimensional numerical model used to generate this plot from Exp-D (Table 2) was initialized using temperature-salinity fields produced in Exp-C for 19 July, 1974, and run for 3 days from rest with no external forcing

Fig. 20 Model-calculated contours of salinity and distributions of horizontal (along transect) and vertical components of density-driven currents along the transect through the Great Bras d'Or Channel (Fig. 1). The contour interval is 1 psu. The distance in the plots is measured from the NE end of transect. The three-dimensional numerical model used to generate this plot from Exp-D (Table 2) was initialized using temperature-salinity fields produced in Exp-C for 19 July, 1974, and run for 3 days from rest with no external forcing

Fig. 21 Model-calculated contours of salinity and distributions of horizontal (along transect) and vertical components of density-driven currents along the transect through the Barra Strait (Fig. 1). The contour interval is 1 psu. The distance in the plots is measured from the NE end of transect. The three-dimensional numerical model used to generate this plot from Exp-D (Table 2) was initialized using temperature-salinity fields produced in Exp-C for 19 July, 1974, and run for 3 days from rest with no external forcing

Fig. 22 Comparison of observed (solid line) and model-calculated (dashed line) filtered (25 h low-pass) depth-mean currents along the channel axis of the Barra Strait in July of 1974. The depth-

mean currents are calculated from results of **a)** Exp-C, and **b)** Exp-S (Table 2). Note that a positive value indicates flow from the ocean to the Bras d'Or estuary and vice versa

Table 1 Freshwater discharge (m^3 s^{-1} km^{-2}) from four major rivers in the Bras d'Or watershed into the Bras d'Or estuary, Cape Breton, Nova Scotia, Canada measured during the summer of 1974 (Water Survey of Canada, 1972), and total discharge from the entire Bras d'Or watershed (m^3 s^{-1}) based on these measurements. Areas of the various catchments (km^2) are shown in square brackets

	May	June	July	August
NE Margaree [368 km^2]	0.1125	0.0560	0.0315	0.0130
SW Margaree [357 km^2]	0.0616	0.0381	0.0201	0.00961
Grand River [120 km^2]	0.0327	0.0252	0.0223	0.00686
Salmon River [199 km^2]	0.0270	0.0111	0.0134	0.00668
Gauged total (m^3 s^{-1} km^{-2})	0.070	0.038	0.023	0.0099
Total flux from the Bras d'Or watershed [3600 km^2] (m^3 s^{-1})	252.0	136.8	82.8	35.8

.

Table 2 List of numerical experiments driven by different combinations of tides (M2), wind forcing (WF), buoyancy forcing associated with freshwater input from 17 rivers (FI), heat flux (HF), and sub-tidal sea level variations (η_s)

Index	Name of run	Model dynamics	External forcing
1	Exp-M2	Barotropic, fully nonlinear	M_2 only
2	Exp-M2-L	Barotropic, fully linear	M_2 only
3	Exp-M2-LM	Barotropic, nonlinear bottom friction	M_2 only
4	Exp-M2-LB	Barotropic, linear bottom friction	M_2 only
5	Exp-W	Barotropic, fully nonlinear	WF only
6	Exp-R	Baroclinic, fully nonlinear	FI only
7	Exp-C (Control Run)	Baroclinic, fully nonlinear	Tides+WF+FI+HF+ η_s
8	Exp-D	Baroclinic, fully nonlinear	None
9	Exp-S	Baroclinic, fully nonlinear	Tides+WF+FI+HF

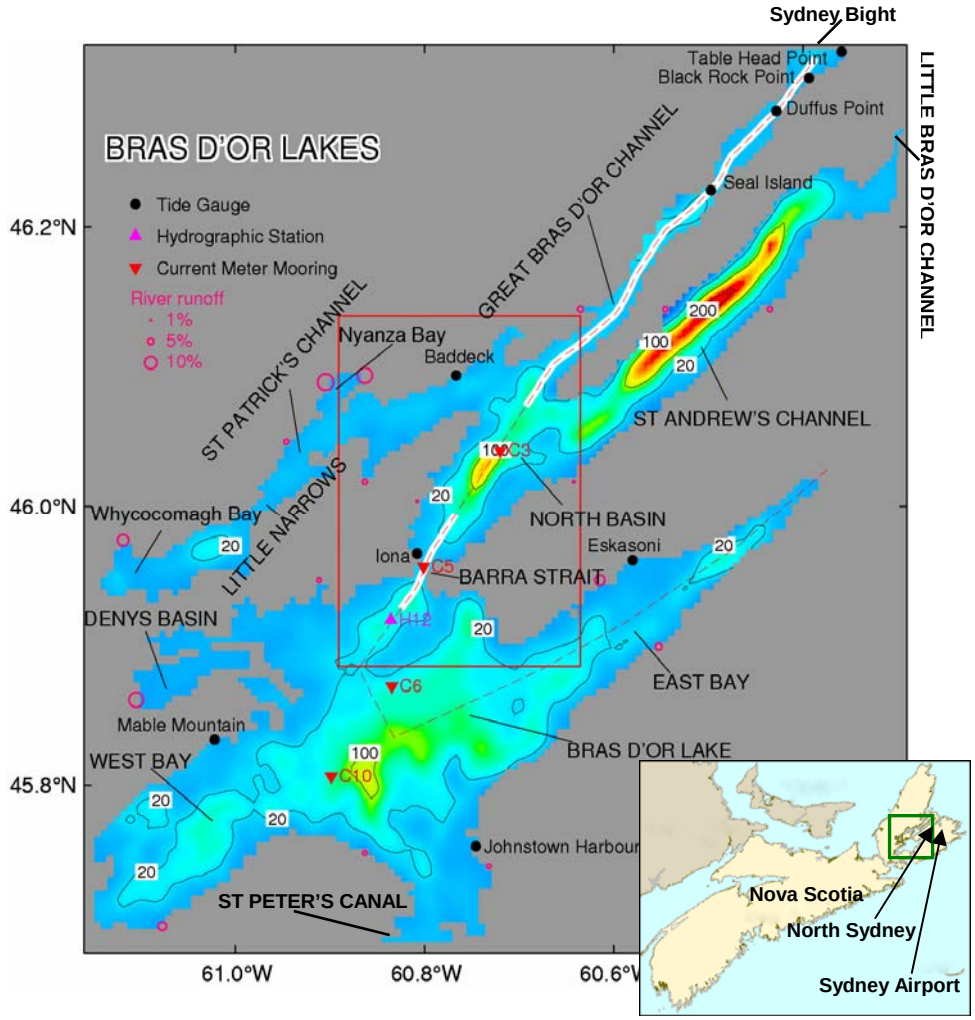

Fig. 1 Map of the Bras d'Or Lakes region of Cape Breton Island, Nova Scotia, Canada, showing selected bathymetric features within the model domain (coloured shading and depths in metres), locations of sea level gauges (solid dots), hydrographic stations (pink triangles) and current meter stations (red triangles). Oceanographic transects through the Great Bras d'Or Channel, North Basin and Barra Strait, where current velocity is presented through the vertical, are marked by thick white lines. Hydrographic transects extending onwards through Bras d'Or Lake and into East Bay, where temperature-salinity data are presented through the vertical, are marked by red dashed lines. The rectangle marked by red solid lines shows the area chosen to present the model-calculated tidal residual flows (Fig. 9). Locations where the mouths of 17 rivers join the model boundary are marked with open red circles. The radius of each circle represents the ratio of freshwater discharge of the river to the total freshwater input to the lake system. Inset shows the location of North Sydney where the tide gauge data were collected, and the Sydney Airport where meteorological measurements were made

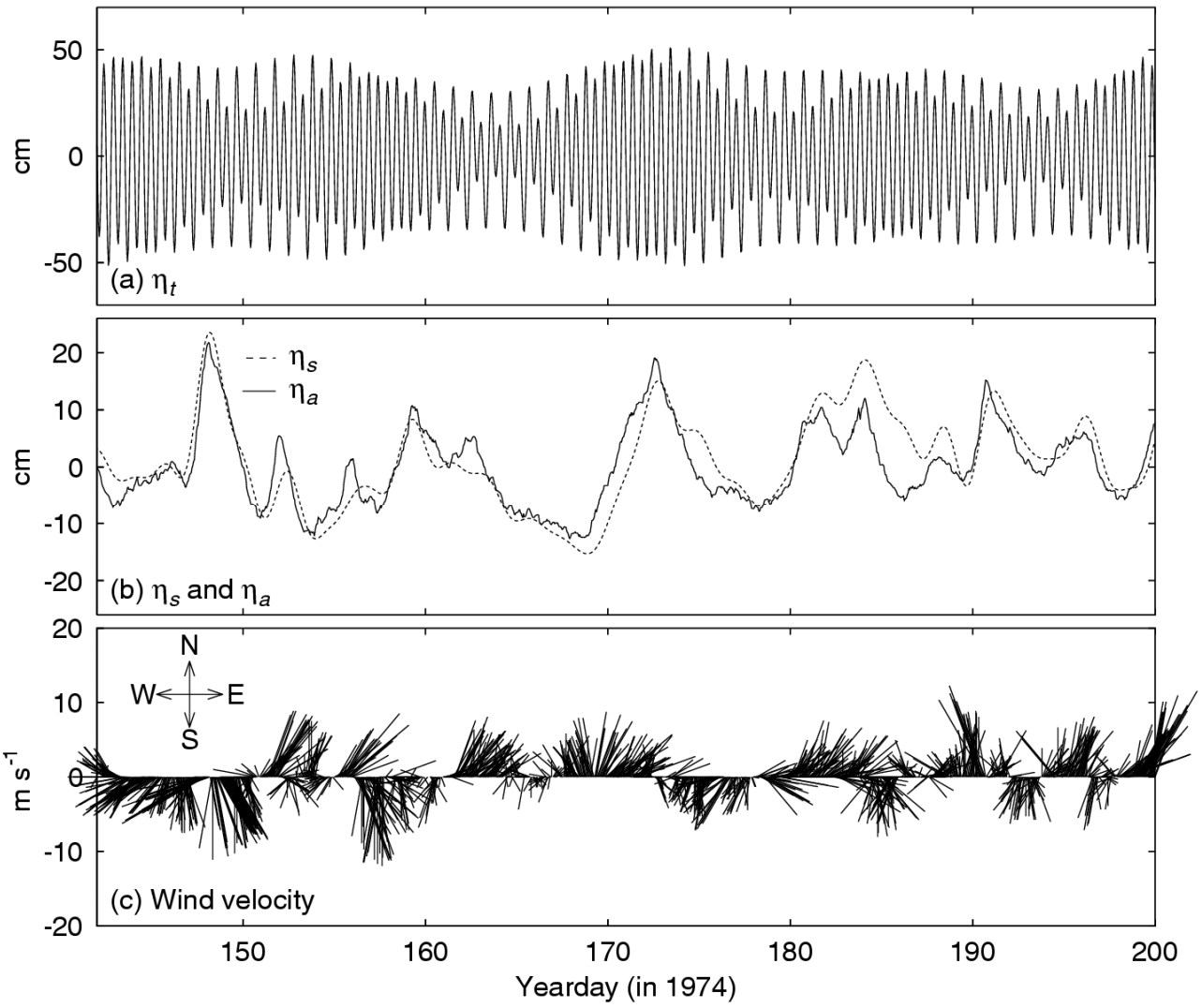

Fig. 2 Empirically measured forcing parameters used in driving a three-dimensional numerical circulation model of the Bras d'Or estuary. Time series of **a)** tidal forcing η_t, **b)** sub-tidal components of the observed sea levels (η_s) at North Sydney and sea level variations due to the inverse barometer effect (η_a) calculated from the air pressure measurements at Sydney Airport, and **c)** observed wind velocity at Sydney Airport during the study period from 00:00 May 23 (day 142) to 00:00 July 20 (day 200) in 1974

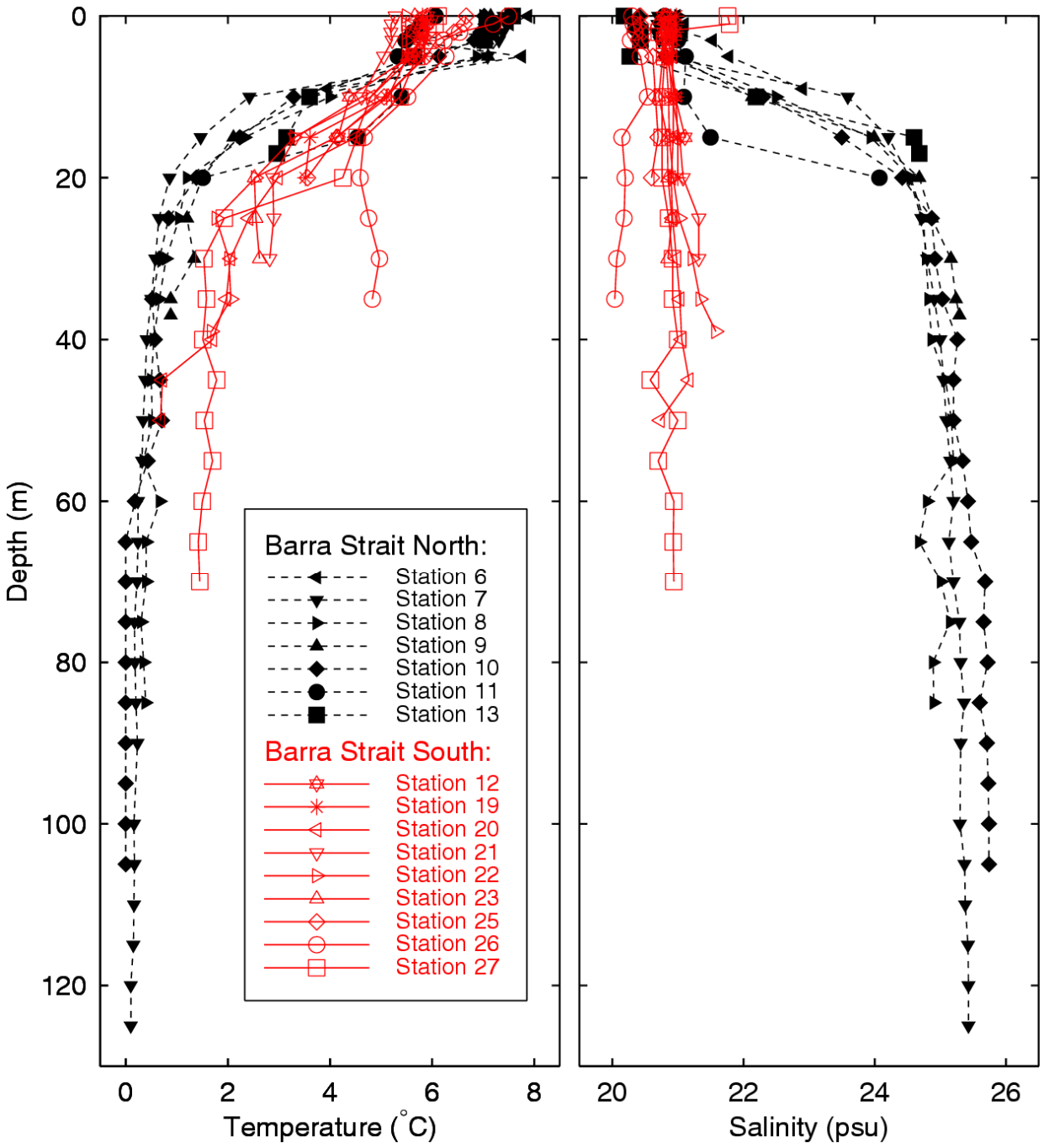

Fig. 3 Vertical profiles of **a)** observed temperatures and **b)** salinities in the Bara Strait separating the two great basins of the Bras d'Or estuary on May 22 and 23, 1974 (See Gurbutt and Petrie 1995 for the hydrographic locations)

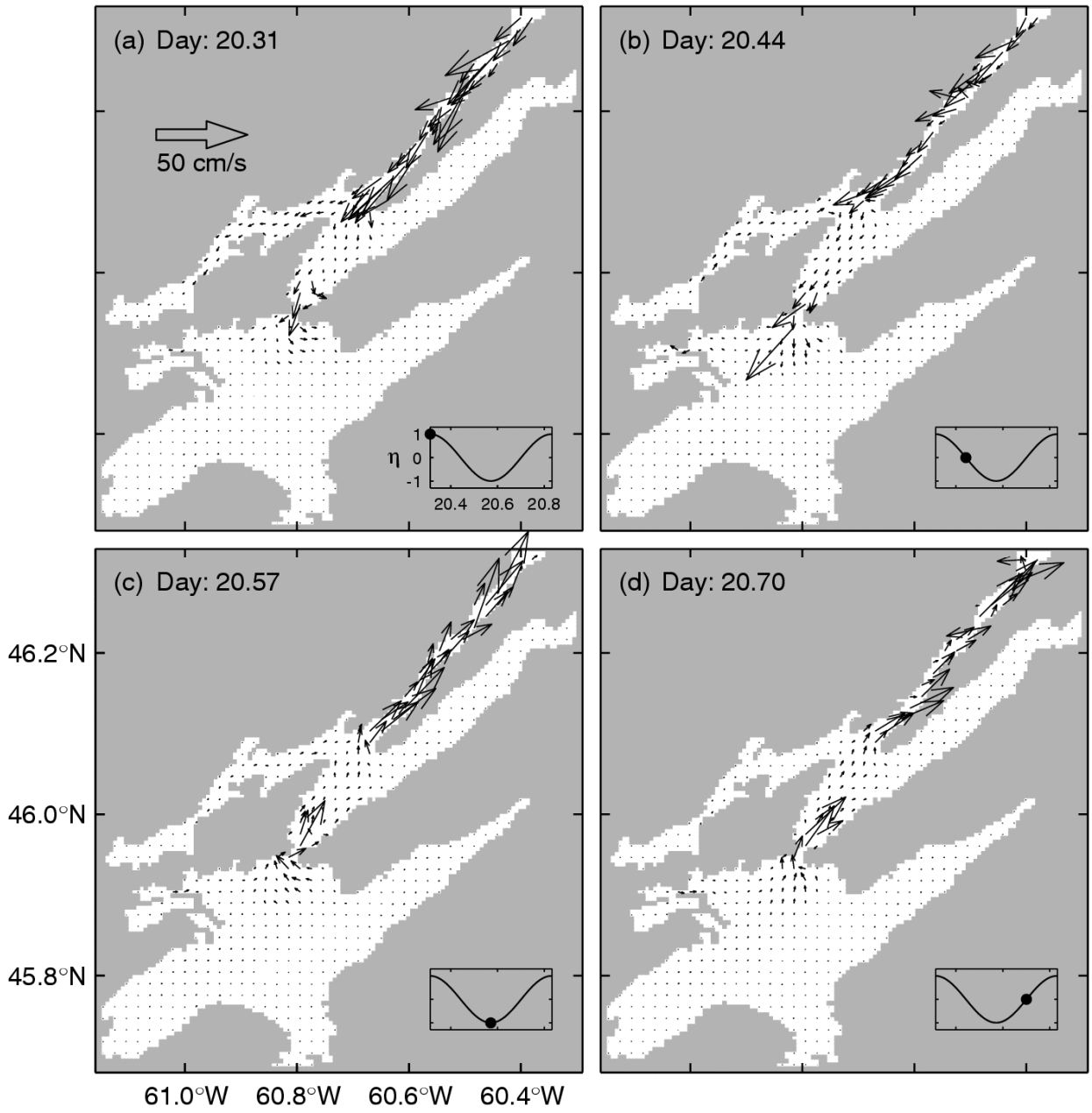

Fig. 4 Near-surface (2 m) currents at four tidal stages in the Bras d'Or estuary (see Fig. 1), produced by the three-dimensional numerical circulation model in Exp-M2 (see Table 2). Current vectors are plotted at every third model grid. The model is forced by the M_2 tidal surface elevations specified at the northern open boundary. Insets show time series of sea levels at the northern open boundary, and the position in the tidal cycle is marked by the solid circle

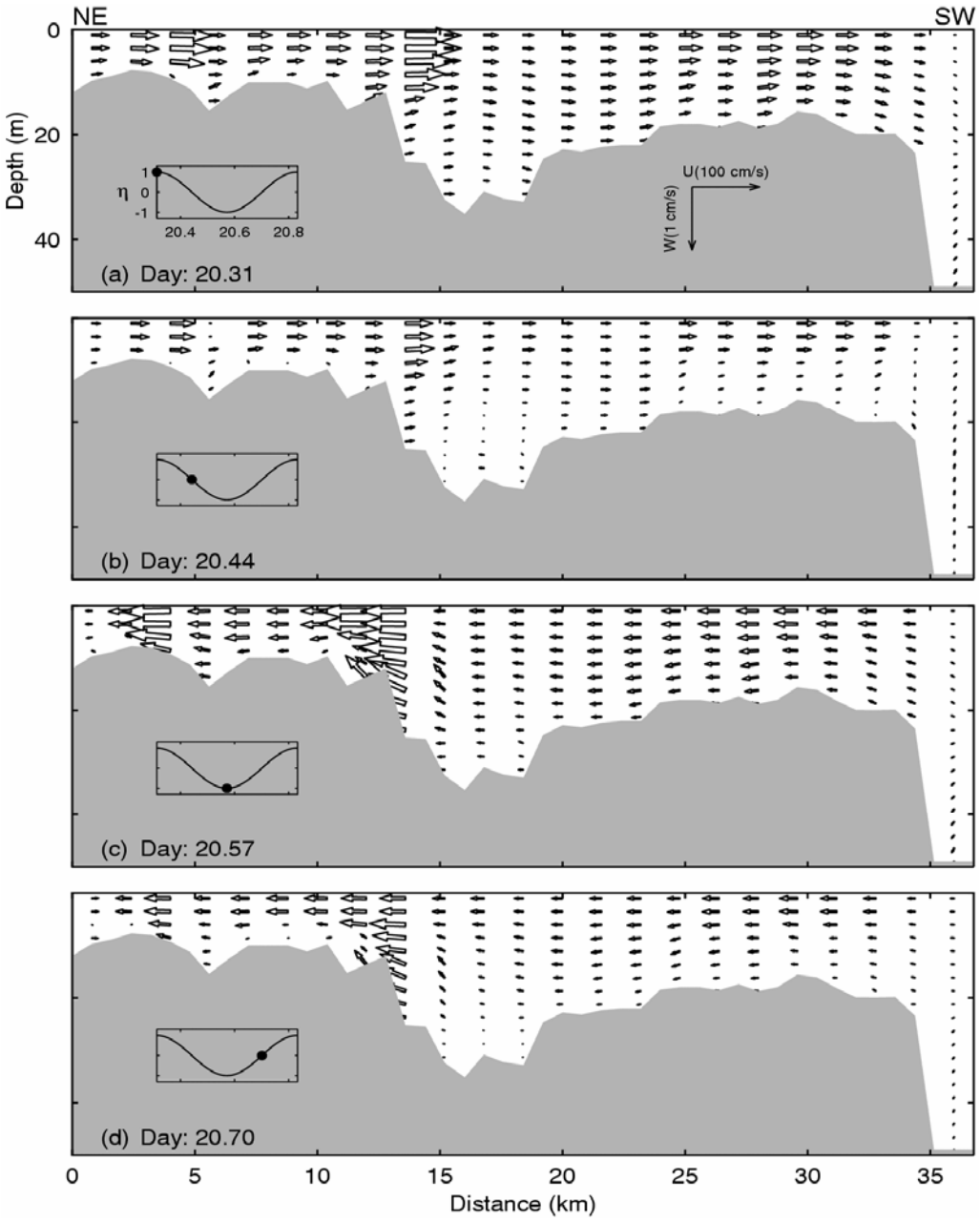

Fig. 5 Distributions of horizontal (along transect) and vertical components of tidal currents along the longitudinal axis of the Great Bras d'Or Channel (Fig. 1), produced by a three-dimensional numerical model in Exp-M2 (Table 2). The distance in the plots is measured from the NE end of transect. The model is forced by the M_2 tidal surface elevations specified at the northern open boundary. Insets show time series of sea levels at the northern open boundary, and the position in the tidal cycle is marked by the solid circle

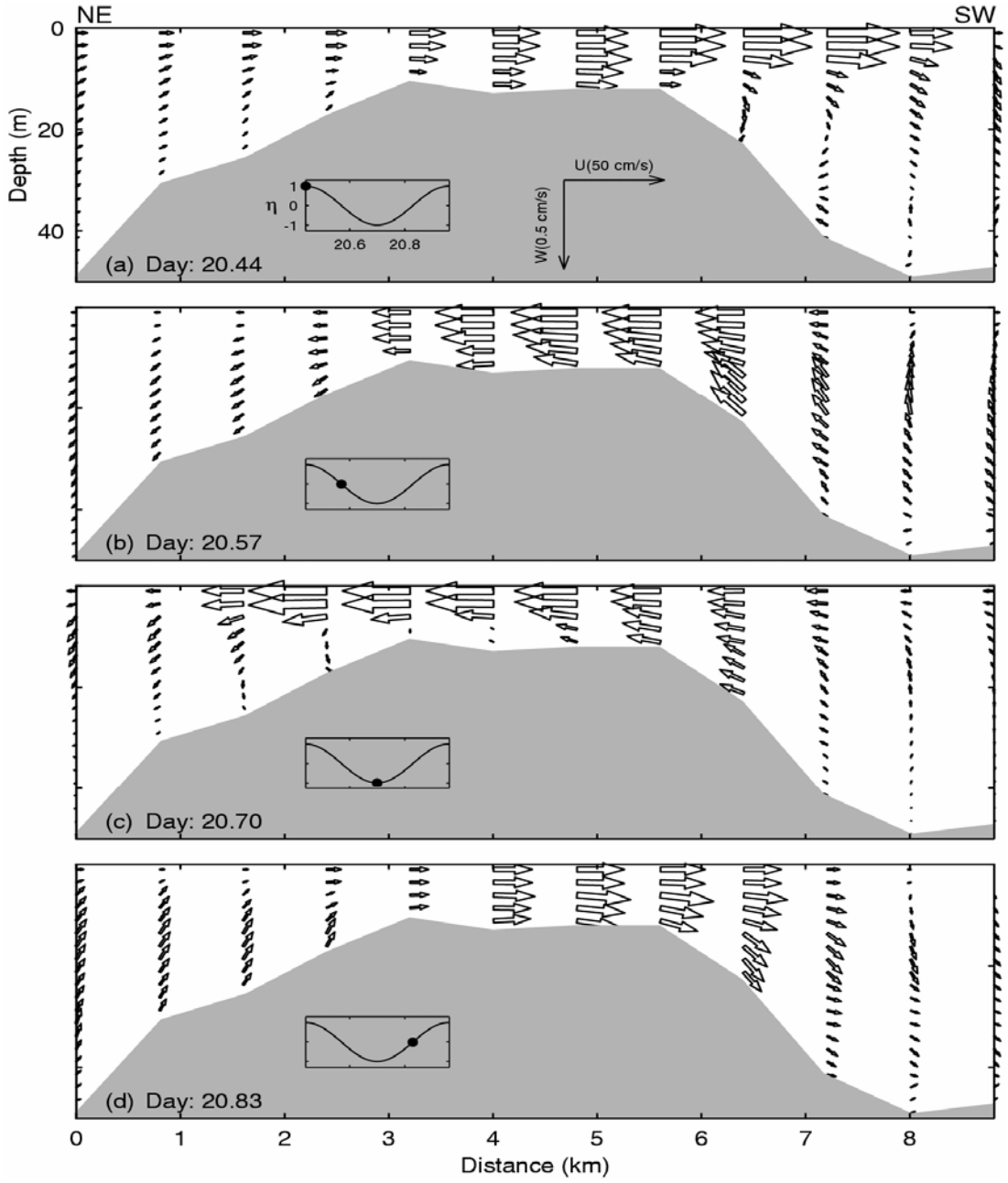

Fig. 6 Distributions of horizontal (along transect) and vertical components of tidal currents along the longitudinal axis of the Barra Strait (Fig. 1), produced by the three-dimensional numerical model in Exp-M2 (Table 2) at four phases of the M_2 tide. The distance in the plots is measured from the NE end of transect. The model is forced by the M_2 tidal surface elevations specified at the northern open boundary of the Great Bars d'Or Channel. Insets show time series of sea levels at the Iona, and the position in the tidal cycle is marked by the solid circle

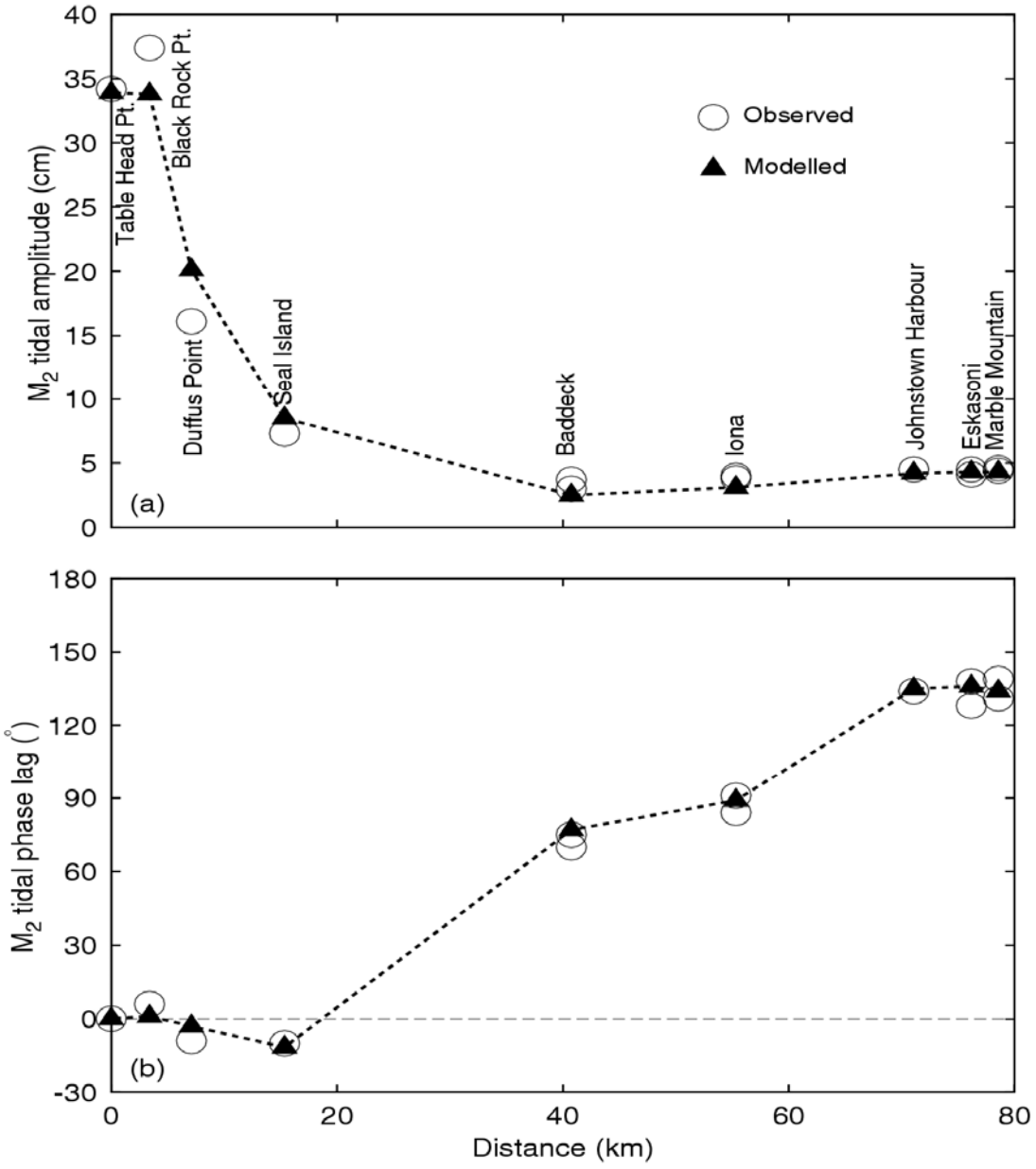

Fig. 7 Comparison of the observed (open circles) and model-calculated (solid triangles) **a)** amplitudes and **b)** phase lags relative to the tidal phase at Table Head Point of the M_2 surface elevations at 9 locations along a transect from the mouth of the Great Bras d'Or Channel to the NE end of West Bay, Bras d'Or estuary (Fig. 1). The model is forced by the M_2 tidal surface elevations specified at the northern open boundary of the Great Bars d'Or Channel. The thin dashed line in **b)** represents zero phase lag

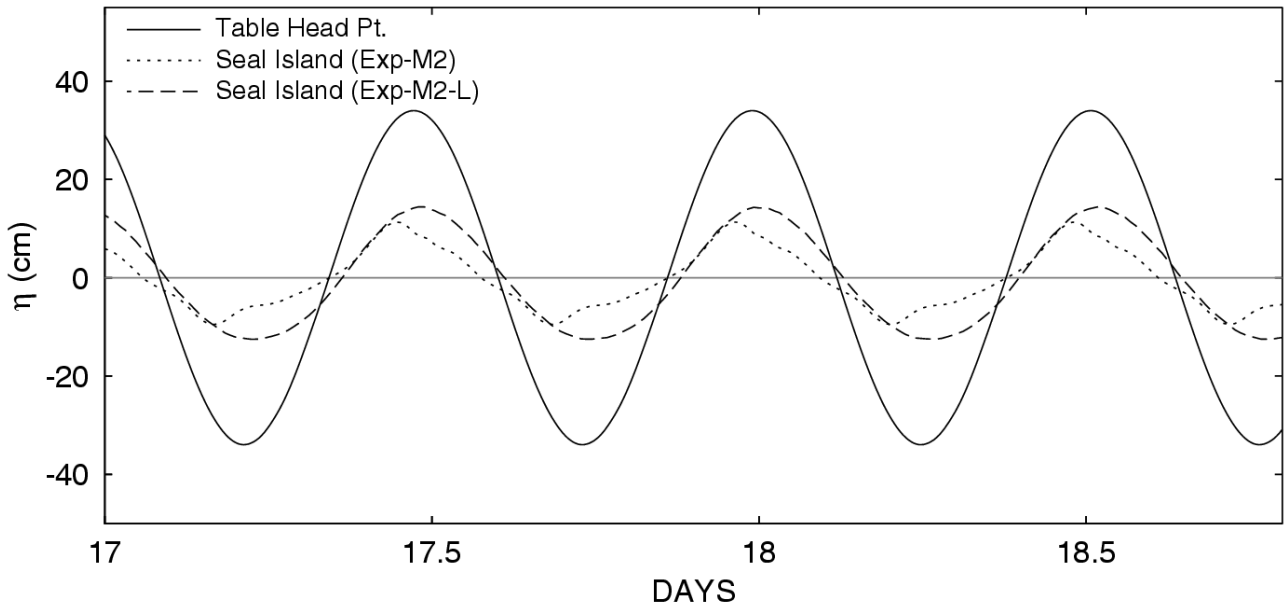

Fig. 8 Time series of surface elevations specified for Table Head Point at the northern open boundary (solid line), and model-calculated surface elevations at Seal Island in Exp-M2 (dotted line) and Exp-M2-L (dashed line). The time mean value is removed from each of the time series. The three-dimensional numerical circulation model used for the two experiments is forced by the M_2 tide at the model's northern open boundary

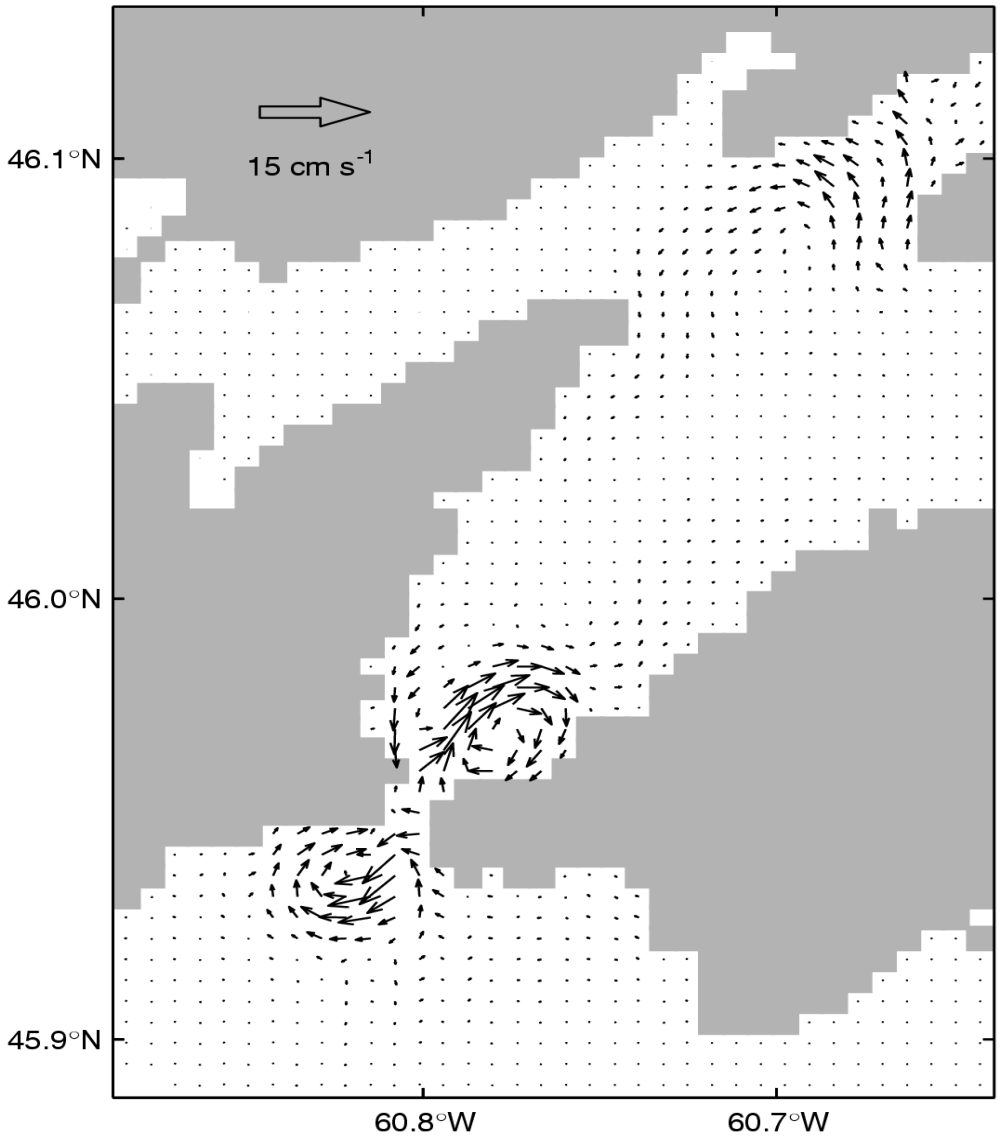

Fig. 9 Near-surface tidal residual flow in the vicinity of the Barra Strait (Fig. 1), as calculated from the model results of Exp-M2 (Table 2). The three-dimensional numerical model is forced by the M_2 tidal elevation specified at the model's open boundary. Current vectors are plotted at every model grid

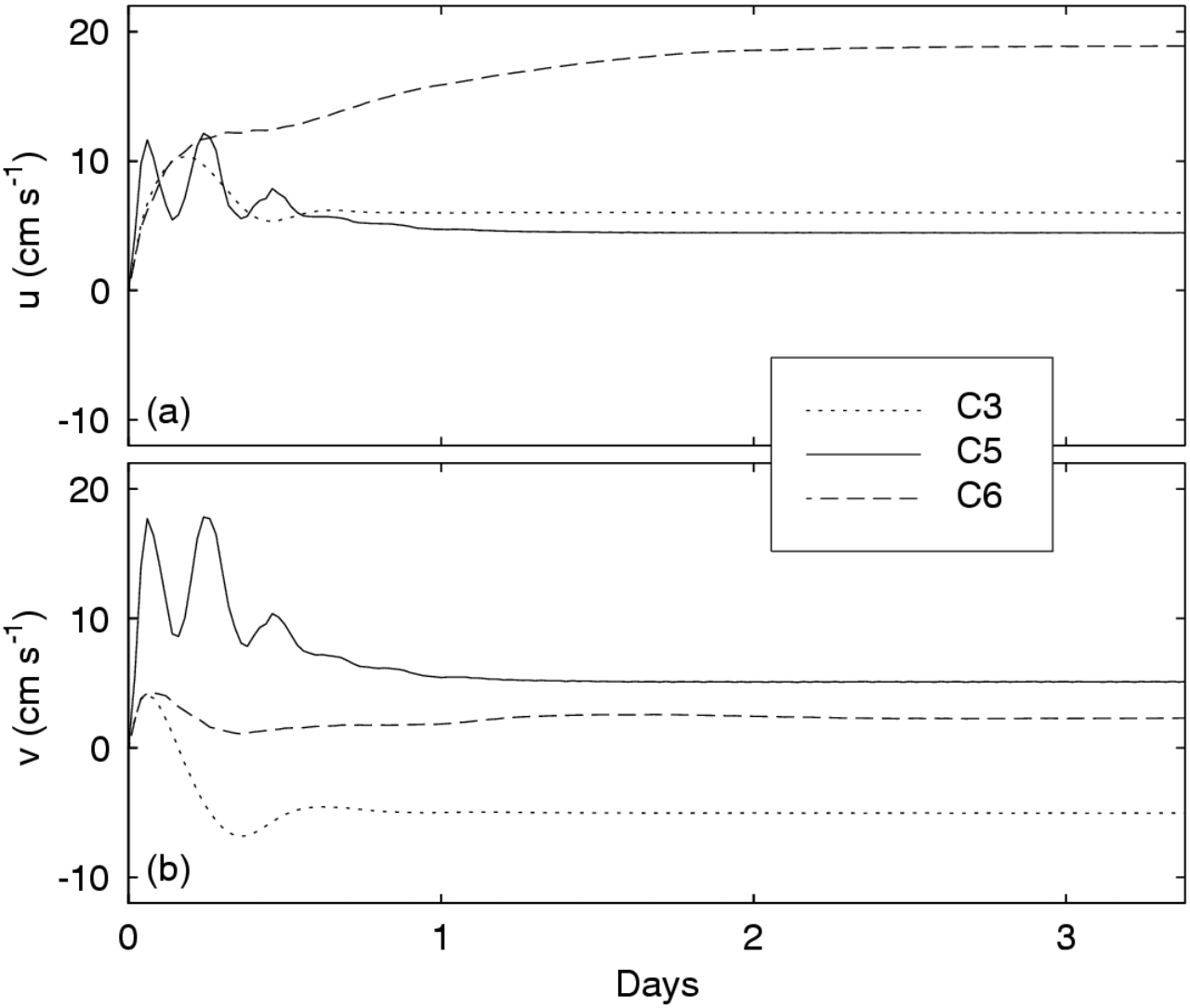

Fig. 10 Time series of **a)** eastward and **b)** northward components of the near-surface currents at locations C3, C5 and C6 along an oceanographic transect from the North Basin to Bras d'Or Lake (Fig. 1), produced by a circulation model in Exp-W (Table 2). The three-dimensional numerical model is forced only by the horizontally uniform and steady northeastward wind velocity of 10 m s^{-1}

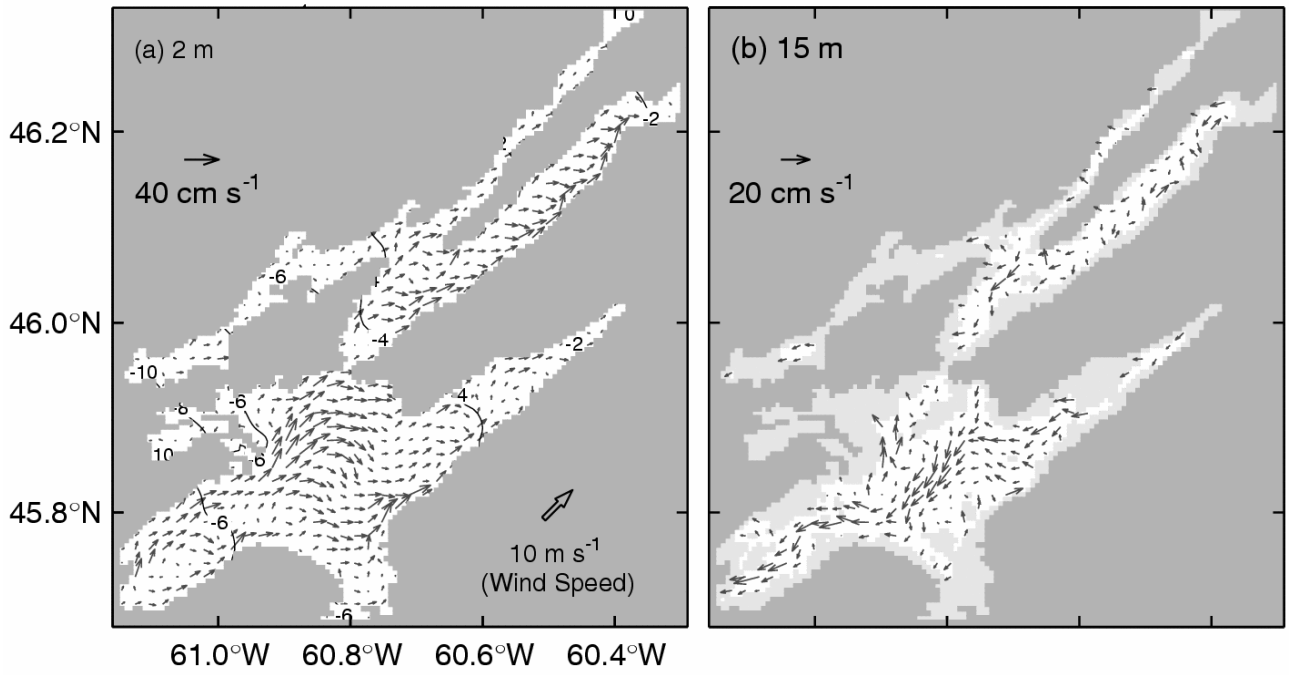

Fig. 11 Model-calculated **a)** surface elevations and near-surface (2 m) currents, and **b)** sub-surface (15 m) currents at day 10 in a barotropic run (Exp-W) of a three-dimensional numerical circulation model of the Bras d'Or estuary (Fig. 1) forced only by steady northeastward winds of 10 m s^{-1}. Contour interval for elevations is 2 cm. Velocity vectors are plotted at every third model grid

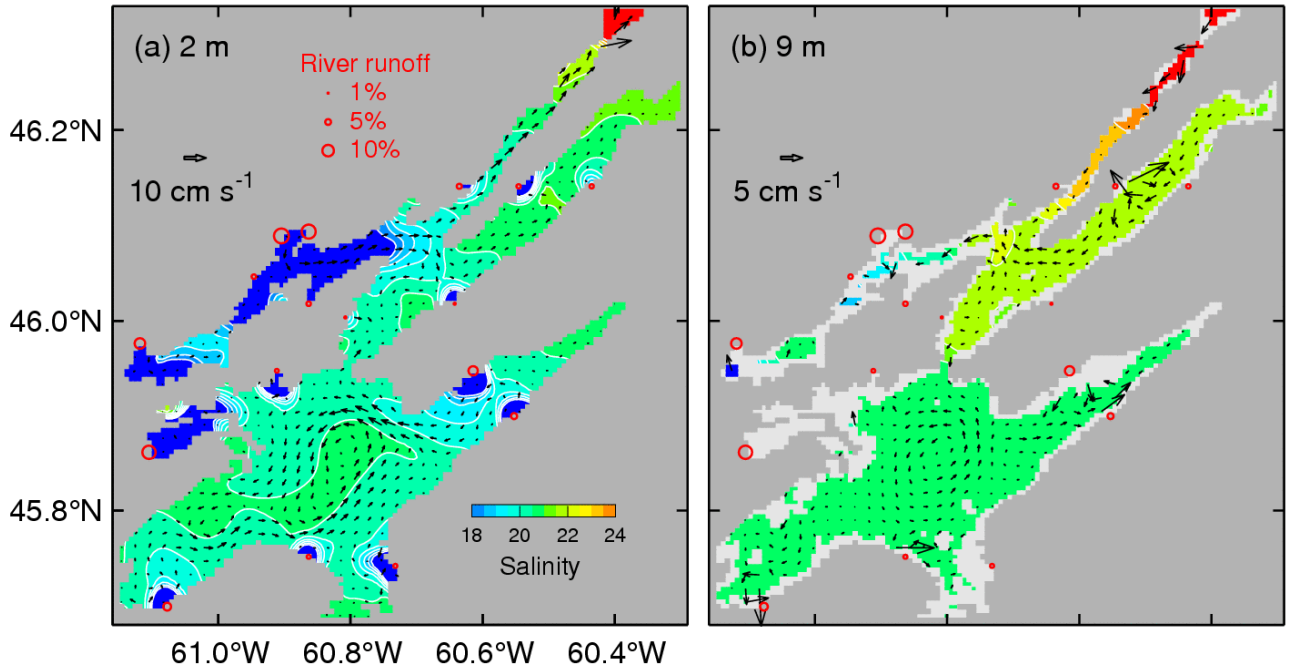

Fig. 12 Model-calculated **a)** near-surface (2 m) currents and salinities, and **b)** sub-surface (9 m) currents and salinities at day 30 in a baroclinic run (Exp-R) of a three-dimensional numerical circulation model of the Bras d'Or estuary (Fig. 1) forced only by steady river runoff (Table 1). Velocity vectors are plotted at every third model grid

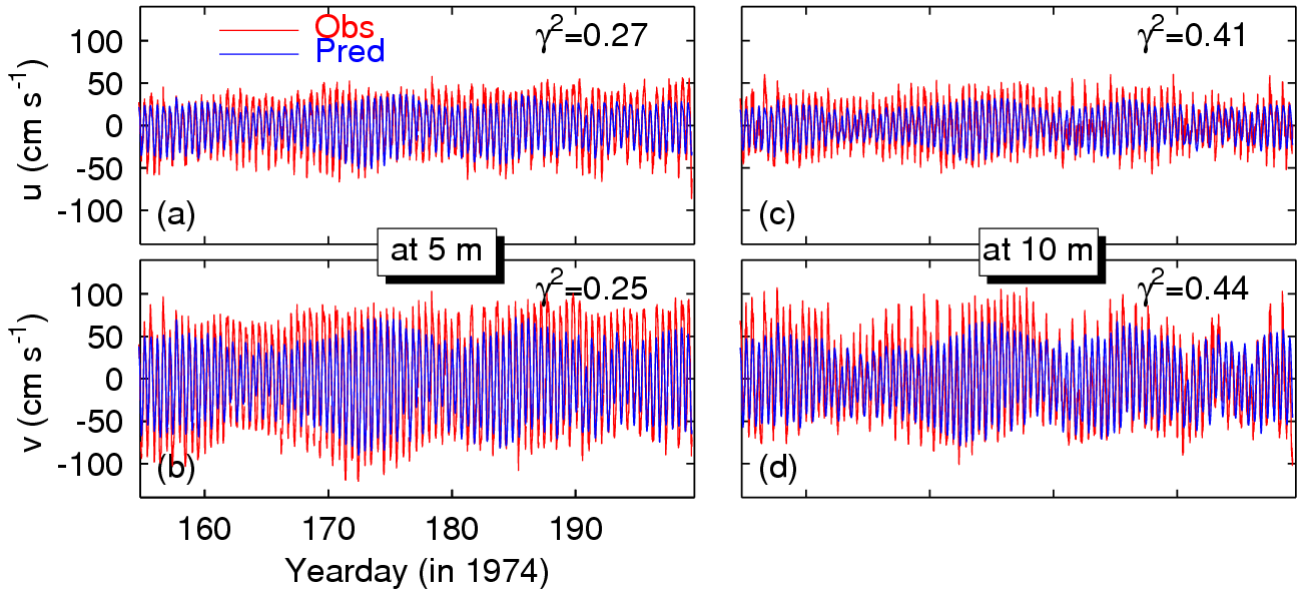

Fig. 13 Time series of scaled (x 1.3), model-predicted (blue plots) and observed (red plots) components of horizontal currents in depths of 5 m (**a** and **b**) and 10 m (**c** and **d**) at site C5 in the Barra Strait during the summer of 1974. The three-dimensional numerical model used for Exp-C (Table 2) was driven by all known forcing (i.e., tides, wind, buoyancy forcing and boundary flows associated with atmospheric pressure perturbations)

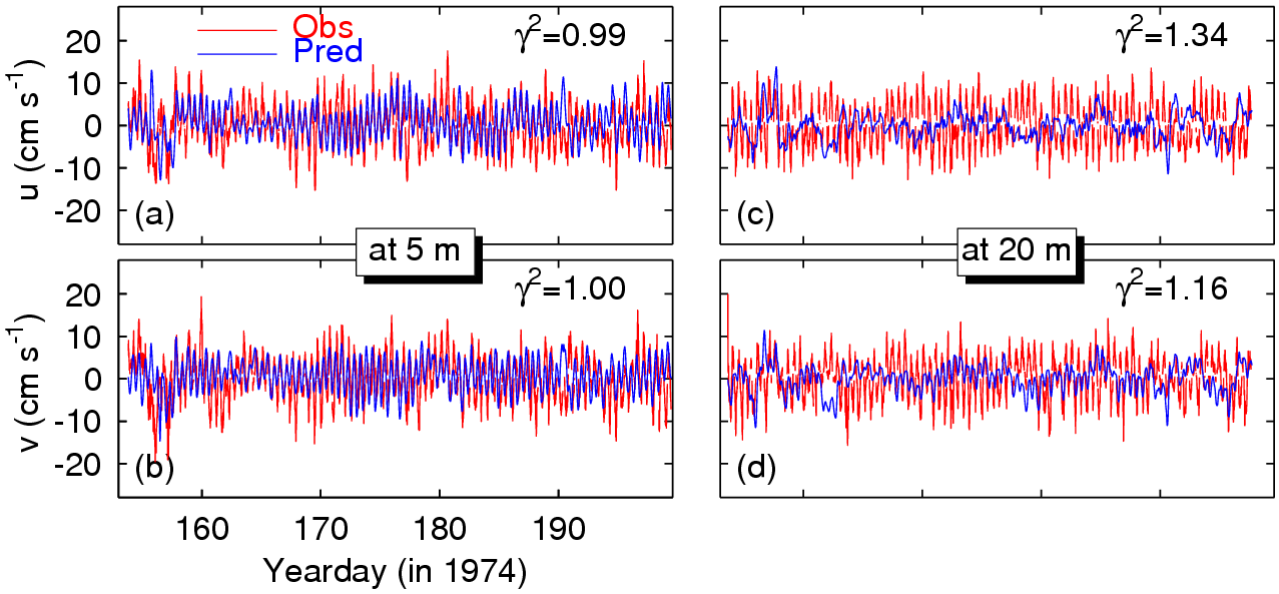

Fig. 14 Time series of model-predicted (blue plots) and observed (red plots) components of horizontal currents in depths of 5 m (**a** and **b**) and 20 m (**c** and **d**), at site C3 in the North Basin of the Bras d'Or estuary during the summer of 1974. The three-dimensional numerical model used for Exp-C (Table 2) was driven by all known forcing (i.e., tides, wind, buoyancy forcing and boundary flows associated with atmospheric pressure perturbations)

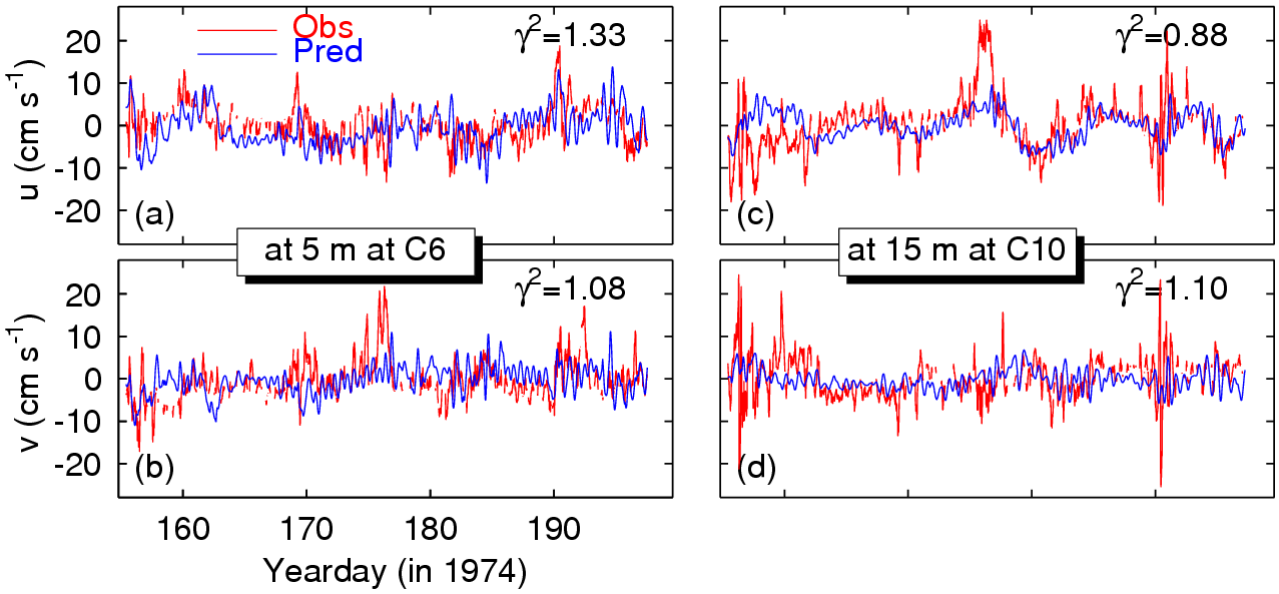

Fig. 15 Time series of model-predicted (blue plots) and observed (red plots) components of horizontal currents in depths of 5 m at site C6 (**a** and **b**) and 15 m at site C10 (**c** and **d**) in Bras d'Or Lake during the summer of 1974. The three-dimensional numerical model used for Exp-C (Table 2) was driven by all known forcing (i.e., tides, wind, buoyancy forcing and boundary flows associated with atmospheric pressure perturbations)

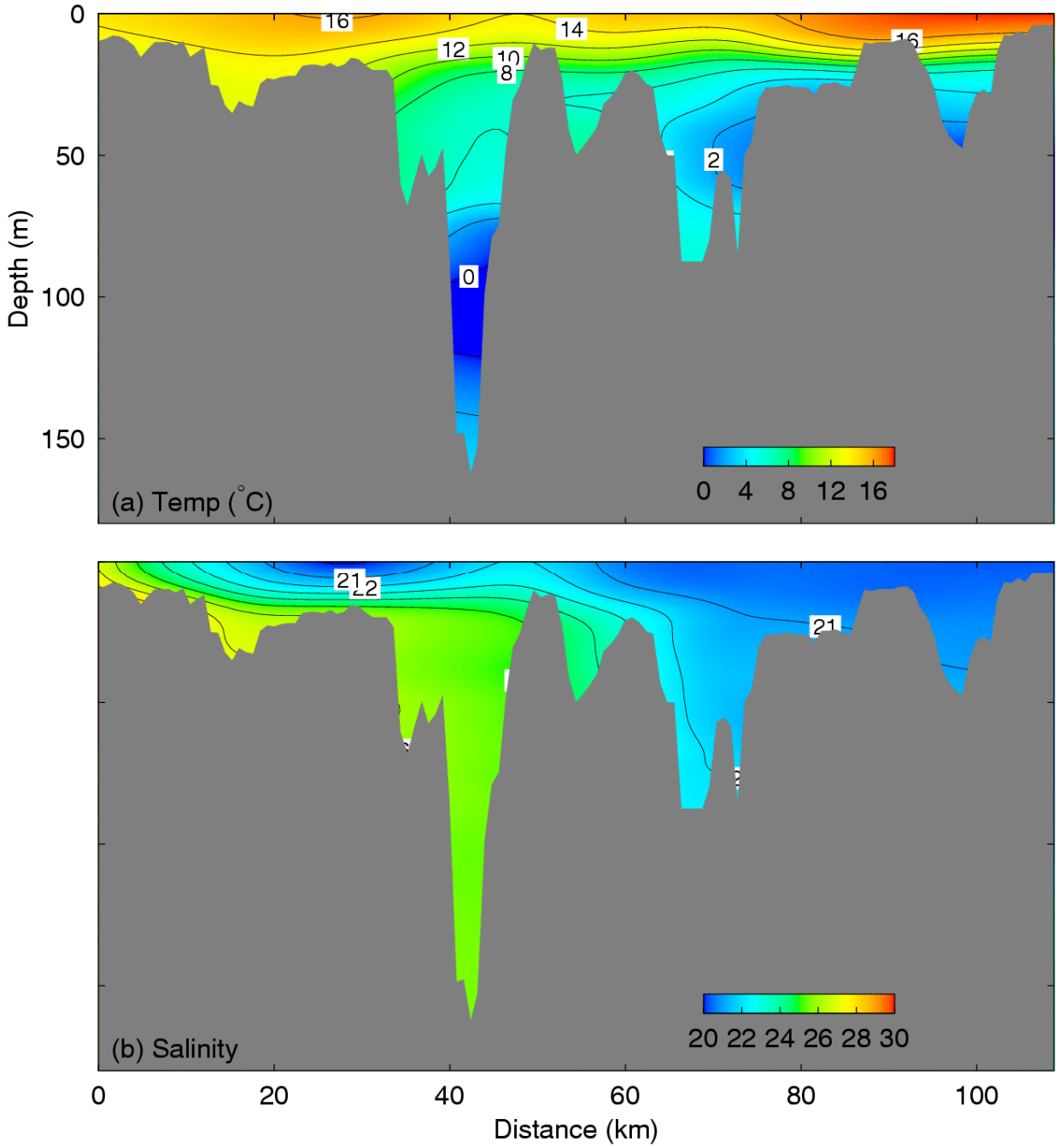

Fig. 16 Observed distributions of **a)** temperature and **b)** salinity along a transect from Table Head Point (left) to the head of East Bay (right) (see Fig. 1) during 15-19 July, 1974 made by Gurbutt and Petrie (1995). The bathymetry of the Great Bras d'Or Channel, North Basin, Barra Strait, Bras d'Or Lake and East Bay are located from left to right. The distance in the plots is measured from the north end of transect

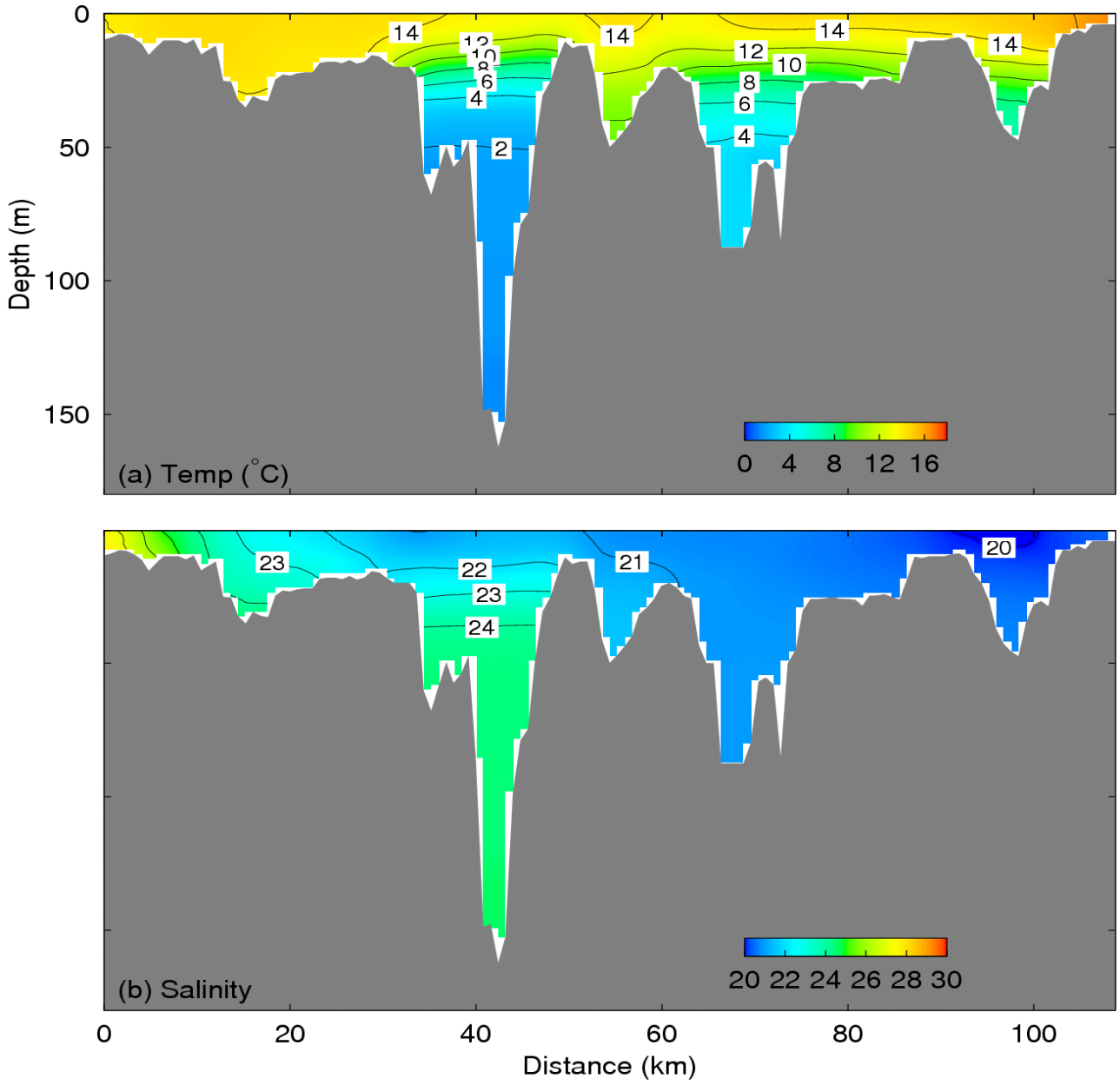

Fig. 17 Model-calculated (Exp-C) time-mean distributions of **a)** temperature and **b)** salinity along a transect from Table Head Point (left) to the head of East Bay (right) predicted for 15-19 July, 1974. The bathymetry of the Great Bras d'Or Channel, North Basin, Barra Strait, Bras d'Or Lake and East Bay are located from left to right. The distance in the plots is measured from the north end of transect. The white areas reflect the coarseness of the model grid scale relative to the resolution of the bathymetry. The three-dimensional numerical model used to generate this plot in Exp-C (Table 2) was driven by all known forcing (i.e., tides, wind, buoyancy forcing and boundary flows associated with atmospheric pressure perturbations)

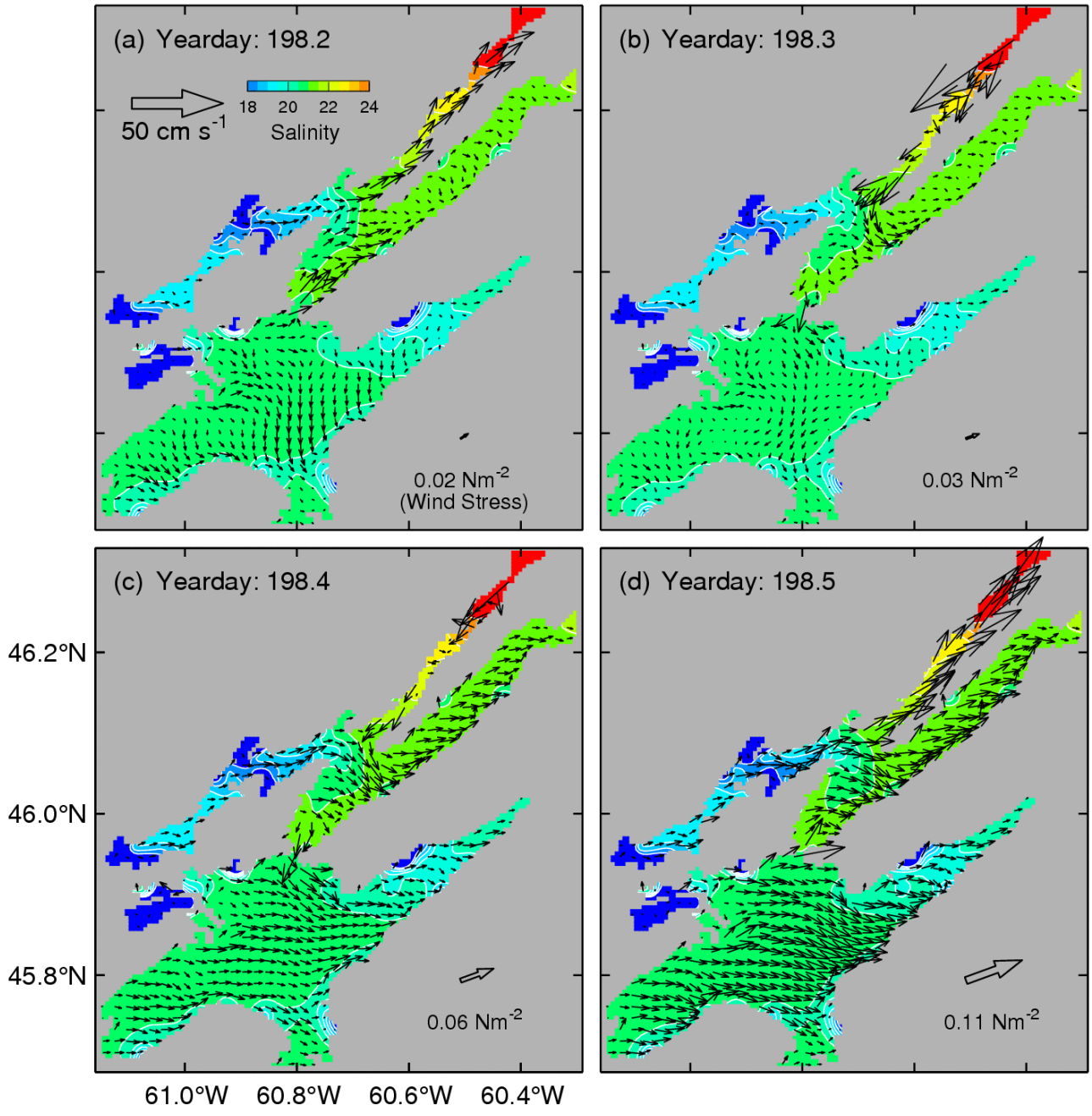

Fig. 18 Model-calculated near-surface (2 m) currents and salinities in the Bras d'Or estuary at four different times during July, 1974. Velocity vectors are plotted at every third model grid. The three-dimensional numerical model used to generate this plot from Exp-C (Table 2) was driven by all known forcing (i.e., tides, wind, buoyancy forcing and boundary flows associated with atmospheric pressure perturbations)

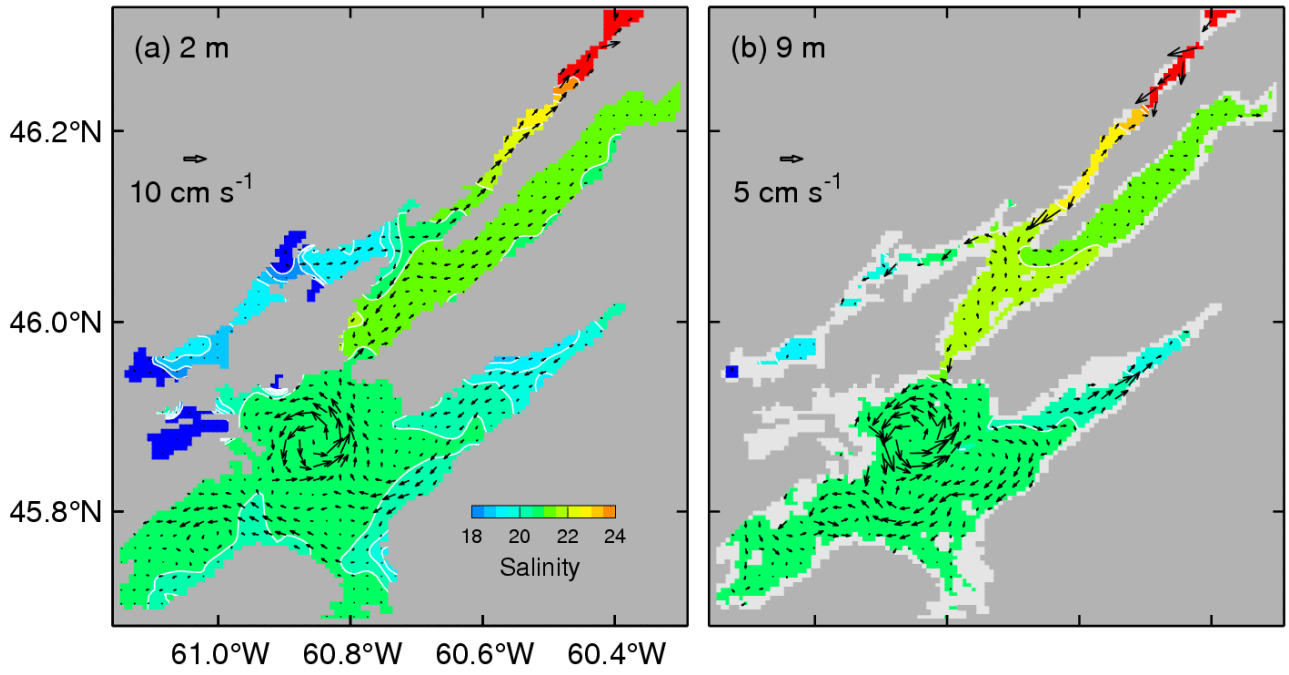

Fig. 19 Model-calculated density-driven currents and salinities in the **a)** near-surface (2 m) layer and **b)** sub-surface (9 m) layer in the Bras d'Or estuary during July, 1974. Velocity vectors are plotted at every third model grid. The three-dimensional numerical model used to generate this plot from Exp-D (Table 2) was initialized using temperature-salinity fields produced in Exp-C for 19 July, 1974, and run for 3 days from rest with no external forcing

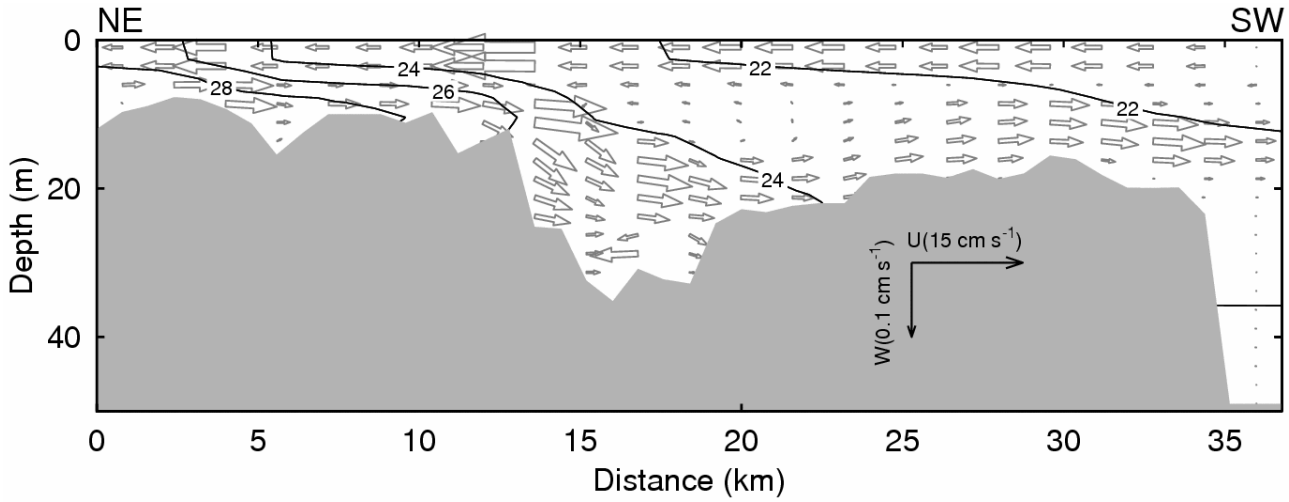

Fig. 20 Model-calculated contours of salinity and distributions of horizontal (along transect) and vertical components of density-driven currents along the transect through the Great Bras d'Or Channel (Fig. 1). The contour interval is 1 psu. The distance in the plots is measured from the NE end of transect. The three-dimensional numerical model used to generate this plot from Exp-D (Table 2) was initialized using temperature-salinity fields produced in Exp-C for 19 July, 1974, and run for 3 days from rest with no external forcing

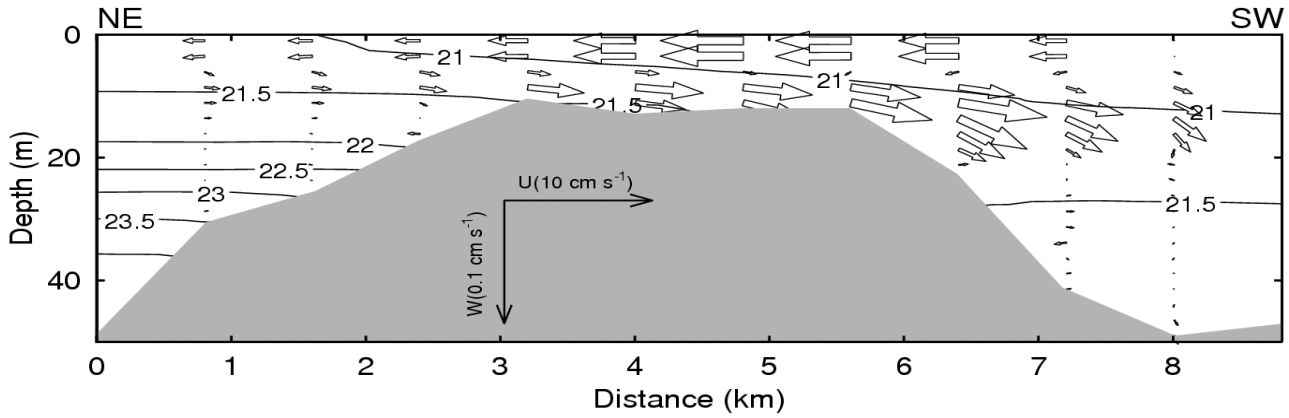

Fig. 21 Model-calculated contours of salinity and distributions of horizontal (along transect) and vertical components of density-driven currents along the transect through the Barra Strait (Fig. 1). The contour interval is 1 psu. The distance in the plots is measured from the NE end of transect. The three-dimensional numerical model used to generate this plot from Exp-D (Table 2) was initialized using temperature-salinity fields produced in Exp-C for 19 July, 1974, and run for 3 days from rest with no external forcing

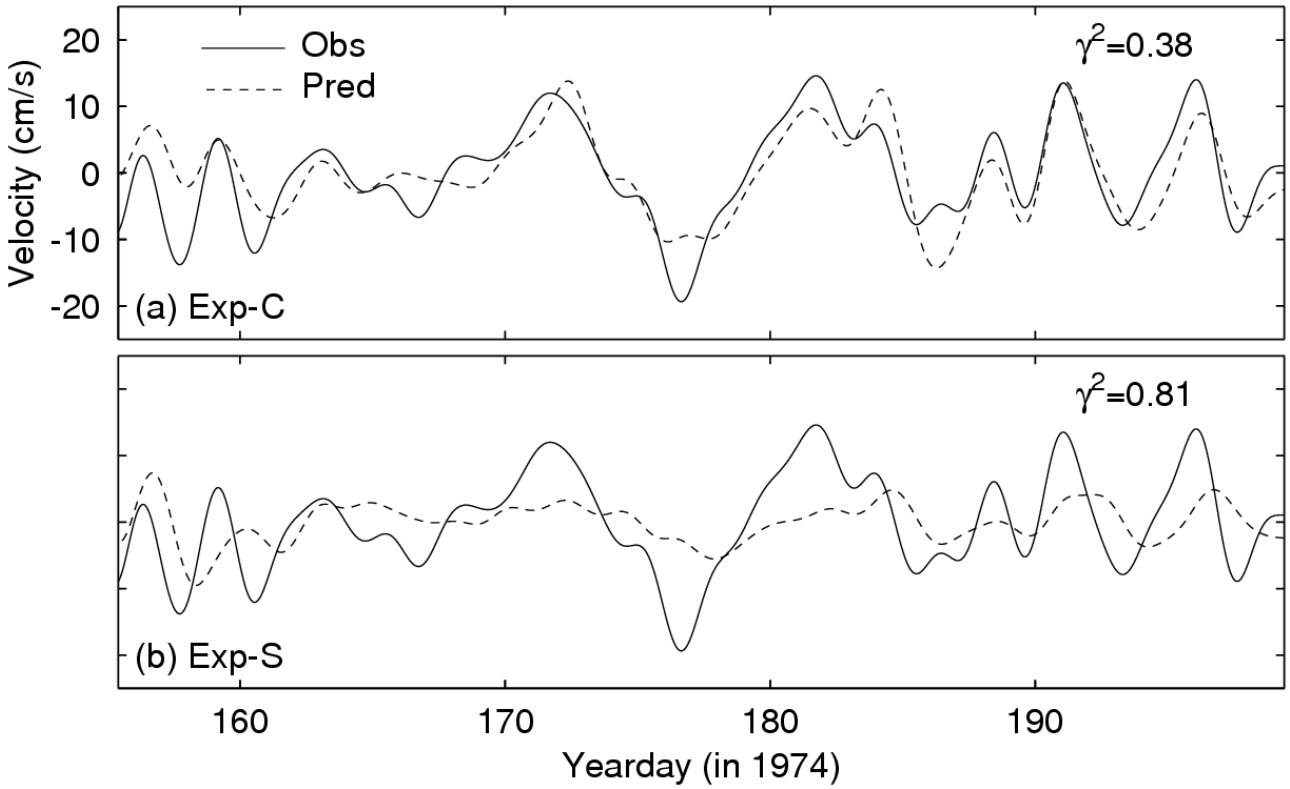

Fig. 22 Comparison of observed (solid line) and model-calculated (dashed line) filtered (25 h low-pass) depth-mean currents along the channel axis of the Barra Strait in July of 1974. The depth-mean currents are calculated from results of **a)** Exp-C, and **b)** Exp-S (Table 2). Note that a positive value indicates flow from the ocean to the Bras d'Or estuary and vice versa